

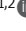




ARTICLE

ER arrival sites associate with ER exit sites to create bidirectional transport portals

Sudeshna Roy Chowdhury^{1,2*}, Chumki Bhattacharjee^{1,2*} , Jason C. Casler³ , Bhawik Kumar Jain^{1,2} , Benjamin S. Glick³ , and Dibyendu Bhattacharyya^{1,2} 

COPI vesicles mediate Golgi-to-ER recycling, but COPI vesicle arrival sites at the ER have been poorly defined. We explored this issue using the yeast *Pichia pastoris*. ER arrival sites (ERAS) can be visualized by labeling COPI vesicle tethers such as Tip20. Our results place ERAS at the periphery of COPII-labeled ER export sites (ERES). The dynamics of ERES and ERAS are indistinguishable, indicating that these structures are tightly coupled. Displacement or degradation of Tip20 does not alter ERES organization, whereas displacement or degradation of either COPII or COPI components disrupts ERAS organization. We infer that Golgi compartments form at ERES and then produce COPI vesicles to generate ERAS. As a result, ERES and ERAS are functionally linked to create bidirectional transport portals at the ER–Golgi interface. COPI vesicles likely become tethered while they bud, thereby promoting efficient retrograde transport. In mammalian cells, the Tip20 homologue RINT1 associates with ERES, indicating possible conservation of the link between ERES and ERAS.

Introduction

Coat protein complex I (COPI) plays an established role in recycling components from the Golgi to the ER. Resident ER proteins occasionally escape from the ER and are subsequently retrieved from the Golgi or the ER–Golgi intermediate compartment (ERGIC) in retrograde COPI vesicles (Szul and Sztul, 2011). Some transmembrane ER proteins contain cytosolically oriented C-terminal KKxx signals, which are recognized by the COPI for retrieval to the ER (Cosson and Letourneur, 1997). COPI also retrieves transmembrane ER proteins that contain arginine-based retrieval signals (Michelsen et al., 2007) as well as transmembrane ER proteins that associate with the Rer1 recycling factor (Sato et al., 2001). Finally, COPI plays a role in retrieving the KDEL/HDEL receptor (Orci et al., 1997), which captures escaped luminal ER proteins.

Much less is known about the sites at which retrograde COPI vesicles deliver their cargo to the ER. Anterograde COPII vesicles form at specialized ER domains known as ER exit sites (ERES; Budnik and Stephens, 2009; Miller and Barlowe, 2010), and by analogy, it has been proposed that retrograde COPI vesicles are delivered to specific ER arrival sites (ERAS; Spang, 2009). Several studies provide hints that ERES and ERAS may be functionally linked. A live-cell imaging study reported that in mammalian cells, retrograde Golgi-to-ER tubular traffic is directed to ERES (Mardones et al., 2006). This tubule-based

pathway may or may not be related to COPI-dependent retrograde traffic, which likely originates from ERGIC membranes that are proximal to ERES (Hammond and Glick, 2000). More recently, evidence for the existence of ERAS was reported for plant cells (Lerich et al., 2012). That study concluded that plant ERAS are associated with ERES, but the interpretation was somewhat complex because in plant cells, Golgi stacks travel along the ER network and ERES are still incompletely defined (Langhans et al., 2012).

A different perspective was provided by an analysis of COPI-driven Golgi-to-ER traffic in the yeast *Saccharomyces cerevisiae* (Schröter et al., 2016). That study focused on the Dsl1 complex, which recognizes the COPI coat during the capture of COPI vesicles at the ER (Meiringer et al., 2011; Ren et al., 2009; Tripathi et al., 2009). The Dsl1 complex and associated SNAREs were found to be distributed throughout the yeast ER by standard fluorescence microscopy (Meiringer et al., 2011), so as an alternative, the authors used bimolecular fluorescence complementation to identify sites at which COPI interacted with the Dsl1 complex. Their method revealed punctate structures that were interpreted to be ERAS. The punctate structures were not consistently associated with ERES, and instead were concentrated at sites of polarized growth. However, that experimental system is challenging because *S. cerevisiae* contains dozens of

¹Department of Cell and Tumor Biology, Advanced Centre for Treatment Research & Education in Cancer, Tata Memorial Centre, Mumbai, India; ²Homi Bhabha National Institute, Training School Complex, Mumbai, India; ³Department of Molecular Genetics and Cell Biology, The University of Chicago, Chicago, IL.

*S. Roy Chowdhury and C. Bhattacharjee contributed equally to this paper; Correspondence to Dibyendu Bhattacharyya: dbhattacharyya@actrec.gov.in.

© 2020 Roy Chowdhury et al. This article is distributed under the terms of an Attribution–Noncommercial–Share Alike–No Mirror Sites license for the first six months after the publication date (see <http://www.rupress.org/terms/>). After six months it is available under a Creative Commons License (Attribution–Noncommercial–Share Alike 4.0 International license, as described at <https://creativecommons.org/licenses/by-nc-sa/4.0/>).

small ERES as well as nonstacked Golgi cisternae that are scattered throughout the cytoplasm (Rossanese et al., 1999). It seems possible that the dispersed secretory pathway in *S. cerevisiae* is coupled with an unusual arrangement of ERAS.

As a simpler system to study ERAS and their relationship to ERES, we chose the budding yeast *Pichia pastoris*. A typical *P. pastoris* cell contains three to five ERES, each of which is next to a Golgi stack (Rossanese et al., 1999). (We previously referred to ERES in this yeast as transitional ER or tER sites, but are now adopting the ERES term for consistency with other groups.) *P. pastoris* ERES can be labeled by tagging COPII coat subunits with fluorescent proteins and can be tracked by confocal microscopy for tens of minutes. This approach provided the first evidence that ERES are long-lived domains that form de novo and undergo growth, fusion, and shrinkage (Bevis et al., 2002). In addition, *P. pastoris* ERES can be characterized by electron tomography. Those data indicated that an ERES produces multiple COPII vesicles, which accumulate in the space between the ER membrane and the adjacent early cisterna of the Golgi (Levi et al., 2010; Mogelsvang et al., 2003).

Our tomography studies showed that in addition to the COPII vesicles that can be seen budding from *P. pastoris* ERES, smaller vesicles that are presumably COPI vesicles are associated with the ER in close proximity to ERES (Levi et al., 2010; Mogelsvang et al., 2003). It therefore seems plausible that ERES and ERAS form part of an integrated functional unit. To test this idea, we examined the localization and dynamics of the *P. pastoris* Dsl1 complex. Our results are strikingly different from those obtained previously with *S. cerevisiae*. The Dsl1 complex clusters to form ERAS that often take the form of partial rings around ERES, and maintenance of ERAS requires intact ERES as well as active COPI. These data suggest a straightforward mechanistic model for ERAS formation.

Results

The Dsl1 complex localizes to specific domains of the ER

To investigate whether COPI vesicles arrive at specific regions of the ER in *P. pastoris*, we tagged subunits of the Dsl1 complex, which tethers COPI vesicles. The Dsl1 complex consists of Dsl1, Dsl3/Sec39, and Tip20 (Kraynack, 2005). This tether works together with the ER-localized SNARE proteins UfeI, UseI, and Sec20 to capture and fuse retrograde COPI vesicles that travel from the Golgi to the ER (Meiringer et al., 2011). If COPI tethering and fusion occur at distinct ERAS, then the Dsl1 complex should be clustered at domains of the ER.

This prediction was tested by fluorescence microscopy. We tagged the Tip20 and Dsl3 components of the Dsl1 complex with GFP or mCherry. The tagged proteins localized to punctate or ring-like structures (Fig. 1, A and B). When we expressed Tip20-GFP and Dsl3-mCherry in the same strain, the two proteins colocalized almost completely (Fig. 1, B and C). These results suggested that ERAS may indeed exist. To determine whether the labeled puncta were ER domains, we labeled the ER with DsRed-HDEL (Bevis et al., 2002). In a strain expressing DsRed-HDEL and Tip20-GFP, the Tip20 puncta were present on the nuclear envelope and on peripheral ER membranes (Fig. 1 A).

These results indicate that the Dsl1 tethering complex is concentrated at specific ER domains. Based on the further analysis described below, those domains likely represent ERAS.

COPI is closely associated with the Dsl1 complex and is adjacent to ERES

The Dsl1 complex interacts with COPI vesicles and is therefore expected to associate with COPI-labeled structures in vivo. We tested this possibility by tagging Sec26, the β -COP subunit of the COPI coat (Duden et al., 1994). Images from *P. pastoris* strains that coexpressed Sec26-GFP with a Dsl1 complex subunit, either Tip20-mCherry (Fig. 2 A) or Dsl3-mCherry (Fig. S1 A), confirmed that Sec26 colocalized strongly with the Dsl1 complex.

Like the Dsl1 complex, the COPI subunit Sec26 was often visible in structures that resembled partial rings. In the case of COPI, it is plausible that these rings include COPI coats present at Golgi cisternal rims, which are the sites of COPI vesicle budding in mammalian cells (Marsh et al., 2001; Tie et al., 2018) and probably also in *P. pastoris* (Mogelsvang et al., 2003). We therefore labeled the Golgi by tagging two proteins that should be distributed throughout the cisternae: Sec7, a peripheral membrane protein of the late Golgi, and Vig4/Vrg4, an integral membrane protein of the early Golgi (Arakawa et al., 2006; Bevis et al., 2002). Sec26 was adjacent to those Golgi markers and sometimes formed partial or complete rings around the Golgi markers (Fig. S1, B and C). This pattern fits with the assumption that COPI vesicles bud from the rims of Golgi cisternae.

Golgi-derived COPI vesicles become tethered to the ER, and our previous electron tomography studies suggested that those tethered COPI vesicles may be at the periphery of ERES that are producing COPII vesicles (Levi et al., 2010; Mogelsvang et al., 2003). We therefore used fluorescence microscopy to compare the distributions of COPI and COPII components. To label COPII, we tagged the Sec13 coat protein (Bevis et al., 2002). The COPI subunit Sec26 was adjacent to the tightly punctate ERES marked by Sec13 and often partially encircled Sec13 (Fig. 2 B). Three-color imaging of the COPI marker Sec26, the early Golgi marker Vig4, and the ERES marker Sec13 confirmed that all of these components were closely associated, with Sec26 typically in a peripheral location relative to Vig4 and Sec13 (Fig. 2 D). These data support the interpretation that in *P. pastoris* ERES-Golgi units, COPI vesicles bud from the rims of the early Golgi cisternae and then become tethered to the ER at domains that surround the ERES.

ERAS adjoin or encircle ERES and contain ER-localized SNAREs

Because the Dsl1 complex tethers COPI vesicles to the ER, we propose that the ER domains marked by the Dsl1 complex in *P. pastoris* are ERAS. COPI colocalizes with the Dsl1 complex and COPI is adjacent to ERES, so the logical implication is that ERAS should also be adjacent to ERES. To document this point, we constructed *P. pastoris* strains in which ERAS were labeled by tagging Tip20 or Dsl3 with GFP while ERES were labeled by tagging Sec13 with a monomeric DsRed variant (Figs. 2 C and S2 A). As predicted, the ERAS markers were adjacent to ERES and often partially encircled the ERES.

The next question was whether ER-localized SNAREs that mediate fusion of retrograde COPI vesicles also localized to

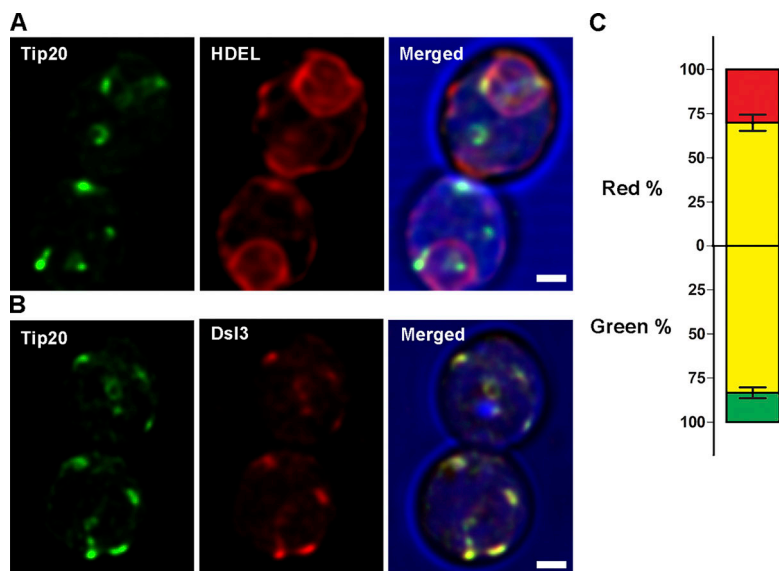


Figure 1. Localization of Dsl1 complex subunits to punctate ER domains in *P. pastoris*. (A) Localization of the Dsl1 complex subunit Tip20. A strain expressed Tip20-GFP together with the general ER marker DsRed-HDEL. Scale bar, 1 μ m. (B) Colocalization of the Dsl1 complex subunits Tip20 and Dsl3. A strain expressed Tip20-GFP and Dsl3-mCherry. Scale bar, 1 μ m. (C) Quantification of the data from B. Colocalization of Tip20-GFP and Dsl3-mCherry was measured for each of \sim 20 individual cells. Above the horizontal axis, yellow indicates the percentage of the red signal that coincided with green pixels, while below the horizontal axis, yellow indicates the percentage of the green signal that overlapped with red pixels. Bars represent SEM.

ERAS. For this purpose, we tagged the Ufel or Sec20 SNARE with GFP in a strain that expressed the DsRed-tagged ERES marker Sec13. The signals from the GFP-tagged SNAREs included background fluorescence that probably reflected localization to the general ER. However, SNARE puncta were also visible and were clearly associated with ERES (Fig. S2, B and C). Moreover, the Sec20 SNARE showed frequent punctate association with the ERAS marker Tip20 (Fig. S2 D). We conclude that ER-localized SNAREs are likely present throughout the ER but can be concentrated in ERAS when the Dsl1 complex links a subset of the ER-localized SNARE molecules to Golgi-associated COPI.

To guide further analysis, we combined the current fluorescence microscopy data with our previous electron tomography data (Levi et al., 2010; Mogelsvang et al., 2003) to generate the working model shown in Fig. 2 E. Early Golgi cisternae are \sim 400 nm in diameter and are tethered to ERES with a gap of \sim 100 nm between the flat surfaces of the ER and Golgi membranes. According to our model, COPI vesicles bud from the rims of early Golgi cisternae. Hence, by diffraction-limited microscopy, COPI appears as a ring-like structure when viewed from the correct orientation. We postulate that the Dsl1 complex binds simultaneously to ER-localized SNAREs and to nascent COPI vesicles, and it remains bound to the COPI vesicles as they undergo scission followed by transfer to the ER surface. Therefore, the Dsl1 complex shows close association with COPI and forms ring-like structures around ERES when viewed from the correct orientation. The estimated length of the Dsl1 complex in association with SNAREs is \sim 70 nm (Travis, S., and F. Hughson, personal communication), suggesting that a Dsl1-SNARE complex could define ERAS by tethering COPI vesicles throughout their life cycle.

ERAS exhibit dynamics similar to ERES

Because ERAS are in close proximity to ERES, we predicted that the dynamics of ERAS would resemble those of ERES. A key question is whether one compartment forms before the other. To address this issue, we performed 4D imaging of the strain in

which ERAS were labeled with Tip20-GFP while ERES were labeled with Sec13-DsRed (Fig. 3 A and Video 1). As previously reported for ERES (Bevis et al., 2002), ERAS formed de novo and gradually increased in size. The formation and expansion of ERAS and ERES structures were tightly linked (Fig. 3 B). Neither compartment appeared to precede the other. Moreover, when ERES fused with one another as previously described (Bevis et al., 2002), the associated ERAS fused as well (Fig. 3 C and Video 2). Similar results were obtained when the fluorescent tags were swapped in a strain expressing Tip20-mCherry and Sec13-GFP (Fig. S3 and Video 3) or when ERAS were marked with Dsl3-mCherry while ERES were marked with Sec13-GFP (Fig. S4, Video 4, and Video 5). These results strengthen the interpretation that ERAS and ERES are tightly linked.

Loss of ERES dramatically affects ERAS

Next, we examined the role of ERES in ERAS formation. Anchoring away the COPII inner layer coat protein Sec23 together with its homologue Shl23 was previously shown to abolish ERES (Bharucha et al., 2013). We therefore constructed a strain expressing FK506 binding protein (FKBP)-tagged ribosomes as well as Sec23-FKBP-rapamycin binding domain (Sec23-FRB), Shl23-FRB, and Tip20-GFP. Addition of rapamycin caused the FRB-tagged proteins to be tethered to ribosomes within 5–10 min (Bharucha et al., 2013). Concomitantly, the ERAS marker Tip20 showed a pronounced and statistically significant reduction in punctate labeling (Fig. 4, A and B). The fluorescence pattern suggests that when ERES are eliminated, ERAS components redistribute to the general ER.

To verify the dependence of ERAS on ERES, we employed the auxin-inducible degron (AID) system (Nishimura et al., 2009; Nishimura and Kanemaki, 2014). This approach allows for rapid and reversible degradation of a tagged protein in response to auxin and enables generation of conditional mutants of essential yeast proteins. *P. pastoris* was engineered to express *Oryza sativa* TIR1 (OsTIR1), an auxin-responsive F-box protein that forms a functional SKP1-CUL1-F-box protein ubiquitin ligase able to

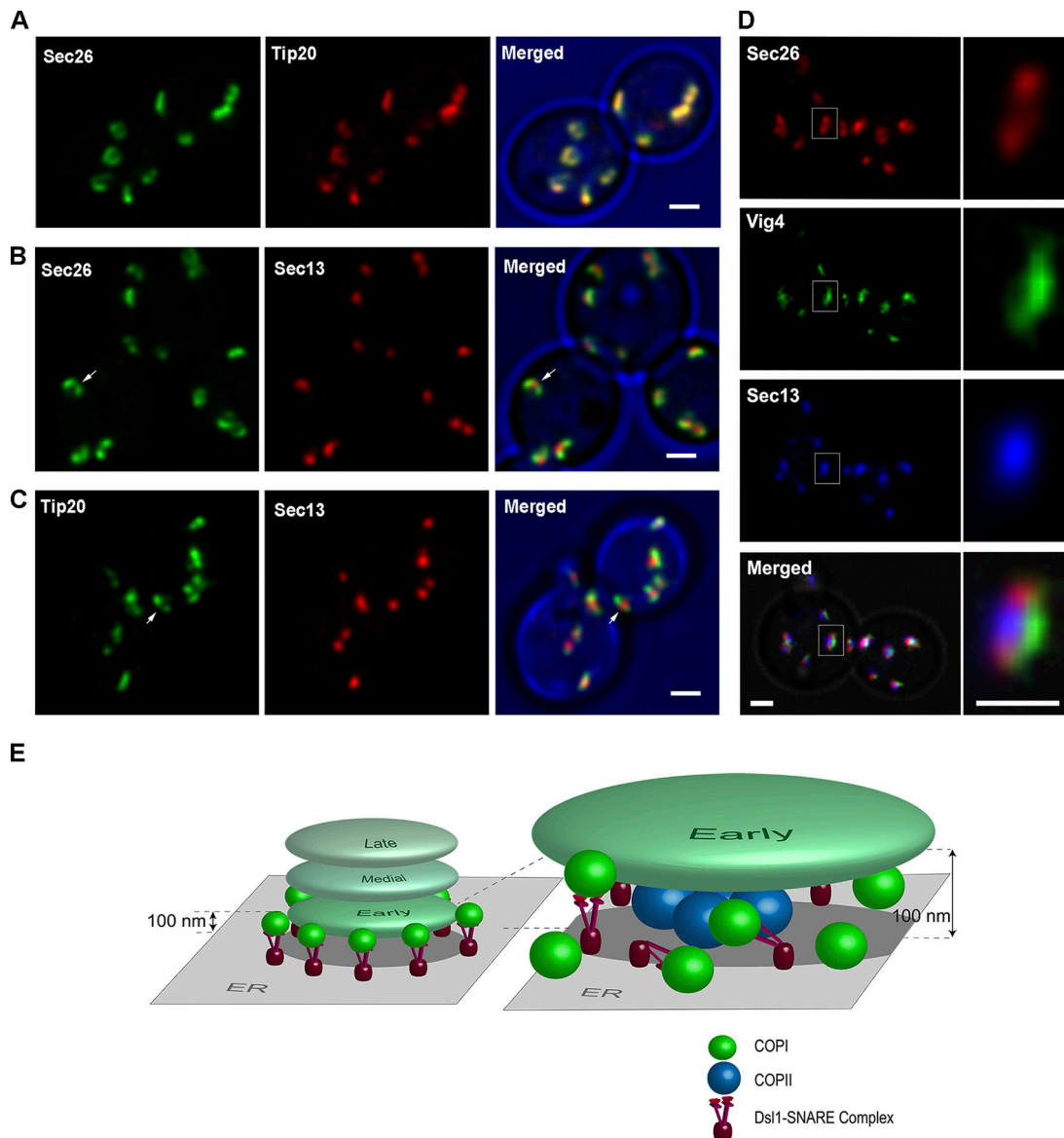


Figure 2. Localization of COPI and ERAS relative to ERES. (A) Colocalization of the COPI marker Sec26 with the ERAS marker Tip20. The strain expressed Sec26-GFP together with Tip20-mCherry. Scale bar, 1 μ m. (B) Adjacent localizations of the COPI marker Sec26 and the ERES marker Sec13. The strain expressed Sec26-GFP together with Sec13-DsRed. The arrow marks a COPI structure that partly surrounds an ERES. Scale bar, 1 μ m. (C) Adjacent localizations of the ERAS marker Tip20 and the ERES marker Sec13. The strain expressed Tip20-GFP together with Sec13-DsRed. The arrow marks an ERAS structure that partly surrounds an ERES. Scale bar, 1 μ m. (D) Relative localizations of the COPI marker Sec26, the early Golgi marker Vig4, and the ERES marker Sec13. The strain expressed Sec26-mCherry, GFP-Vig4, and Sec13-HaloTag. Cells were labeled with JF₆₄₆ before three-color imaging. Scale bars, 1 μ m for the regular images and 0.5 μ m for the magnified insets. (E) Schematic diagram showing the inferred distributions of COPI and COPII vesicles in *P. pastoris* relative to the ER and early Golgi. On the right is an enlarged and more detailed view of the ER–Golgi interface. According to this proposal, as COPI vesicles bud from the rims of early Golgi cisternae, they engage with the Dsl1 complex, which is bound to ER-localized SNAREs. The COPI vesicles ultimately fuse with the ER. Meanwhile, COPII vesicles bud from ERES, each of which lies beneath an early Golgi cisterna. Thus, by fluorescence microscopy, the Dsl1 complex marks ring-like ERAS that colocalize strongly with COPI and surround ERES.

recognize the AID tag derived from *Arabidopsis thaliana* IAA17. OsTIR1 was expressed from the strong constitutive GAP promoter (Sears et al., 1998). The endogenous copy of the COPII inner layer coat protein Sec23 was tagged with three copies of the minimal mini-AID degron (Nishimura et al., 2009; Nishimura and Kanemaki, 2014). As a control, the COPII outer layer coat protein Sec31 was tagged with GFP in a strain expressing Sec23-AID. Within 30 min after addition of auxin

(indole-3-acetic acid [IAA]), the punctate Sec31 signal was lost in most of the cells (Fig. S5, A and B). The experiment was then performed by tagging the ERAS marker Tip20 with GFP in a strain expressing Sec23-AID. After adding IAA, Tip20 dispersed to give a pattern reminiscent of the general ER (Fig. 4, C and D), indicating that loss of ERES also disrupted ERAS. To confirm that Tip20 had redistributed to the general ER, the ER translocon protein Sec63 was tagged with mCherry. After addition of IAA,

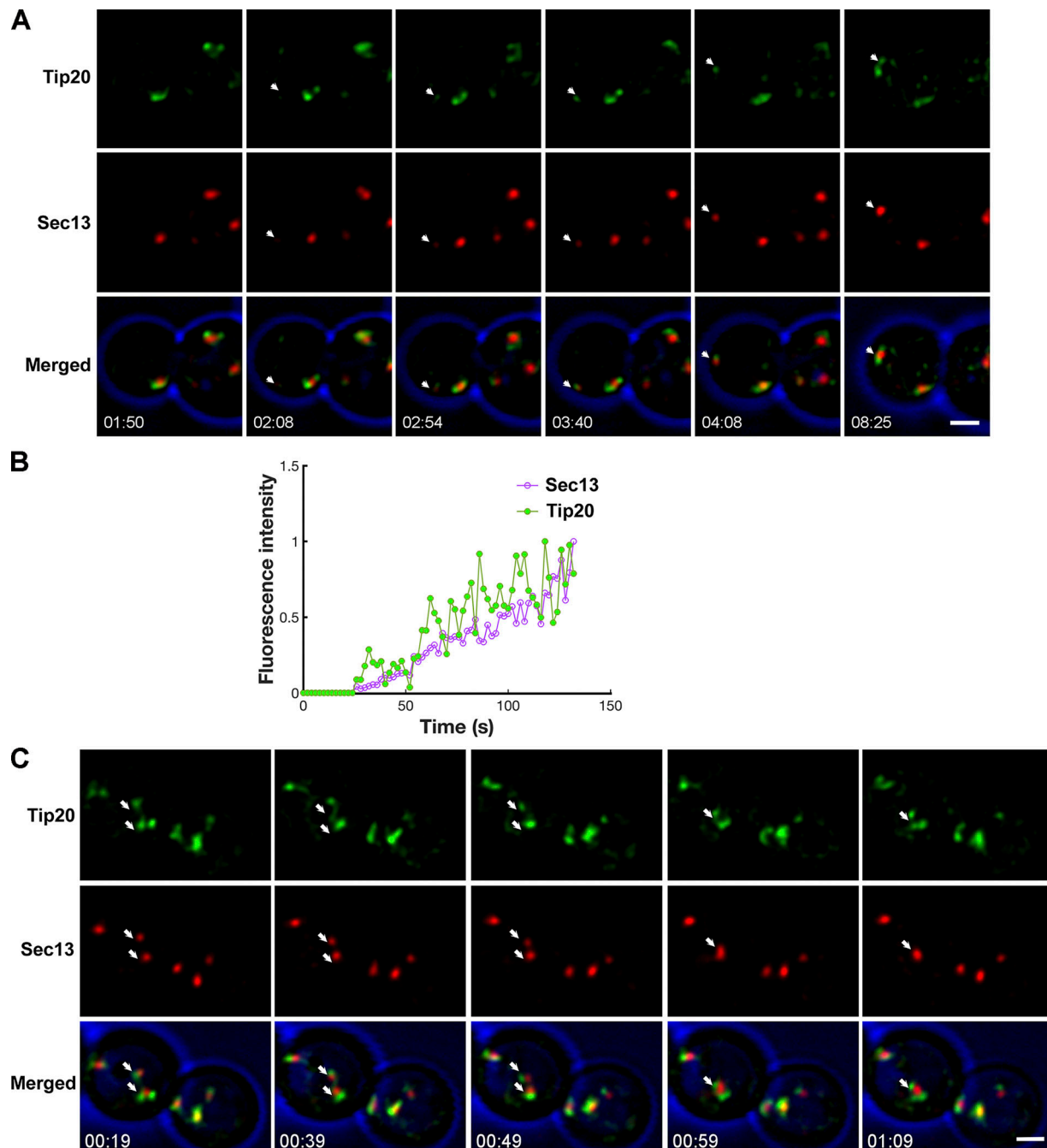


Figure 3. Coupled dynamics of ERAS and ERES. (A) Parallel de novo formation of ERAS structures marked with Tip20 and ERES structures marked with Sec13. A strain expressed Tip20-GFP together with Sec13-DsRed. As marked by the arrows, the coupled formation of a new ERAS and the associated ERES were tracked by 4D confocal microscopy. Shown are frames from [Video 1](#). Scale bar, 1 μ m. **(B)** Quantification of the fluorescence signals from the newly formed structures marked by the arrows in A. Each plot was normalized by setting the highest value to 1. Compared with the Sec13-containing structures, the Tip20-containing structures were more variable and dynamic in shape, so the quantification for Tip20 was noisier. **(C)** Parallel fusion of ERAS and ERES structures. The procedure was as in A, except that the arrows mark two ERAS-ERES pairs that fused to form a single ERAS-ERES pair. Shown are frames from [Video 2](#). Scale bar, 1 μ m.

there was substantial colocalization of the dispersed Tip20 with Sec63 ([Fig. S5 C](#)). These results indicate that the existence of punctate ERAS requires the presence of ERES.

Perturbation of COPI function disrupts ERAS

The next question was whether inactivation of COPI affects ERAS. First, we anchored away the COPI subunit Sec26 in a

strain expressing the ERAS marker Tip20-GFP. There was a dramatic effect on the localization of Tip20, which redistributed to the general ER soon after addition of rapamycin ([Fig. 5 A](#)). Second, we degraded Sec26 using the AID system in a strain expressing Tip20-GFP. By 30 min after addition of IAA, Tip20 had redistributed to the general ER ([Fig. 5, B and C](#)). A control experiment tested whether inactivation of COPI alters ERES.

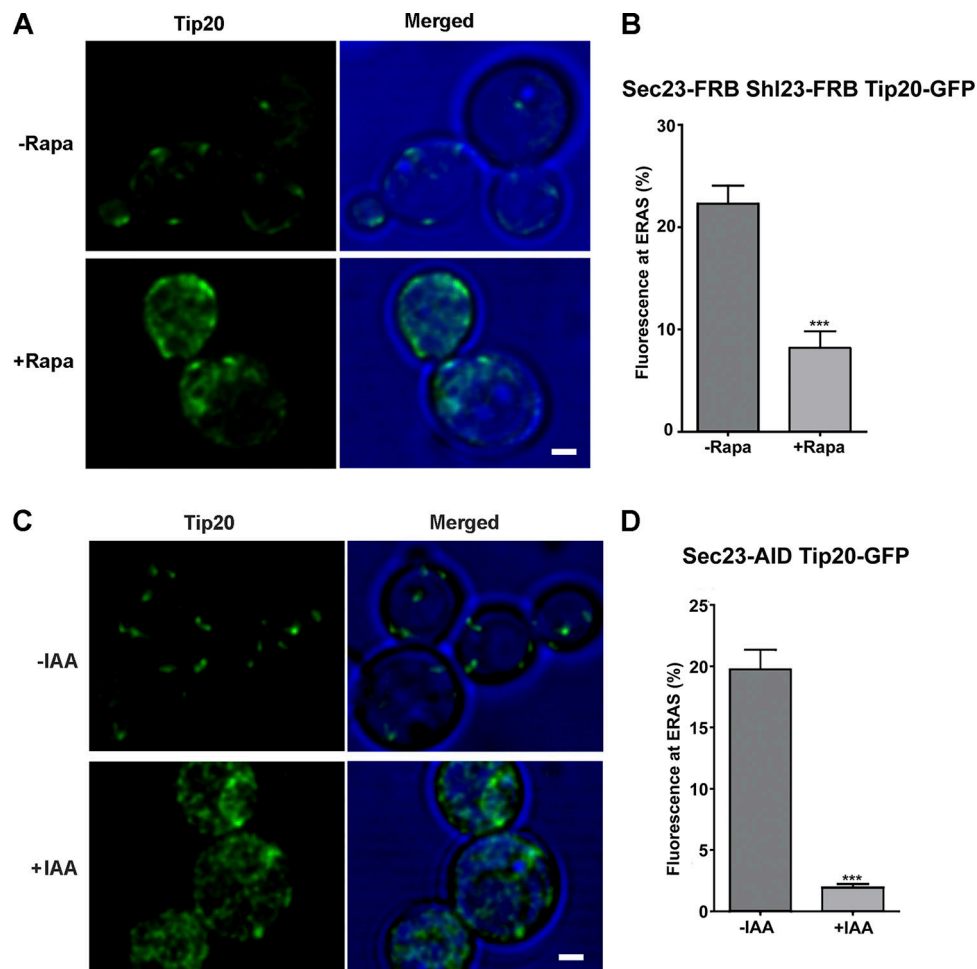


Figure 4. Effect on ERAS of disrupting ERES. (A) Distribution of the ERAS marker Tip20 before and after anchor-away of the ERES components Sec23 and Shl3. A strain expressed Tip20-GFP together with the Rpl17-FKBPx4 ribosomal anchor as well as Sec23-FRB and Shl23-FRB. Images were captured before and after treatment with rapamycin (Rapa) for 10 min. Scale bar, 1 μ m. (B) Quantification of the data from A. The percentage of the total GFP signal that was present at punctate ERAS was measured for ~30 individual cells in each sample. Bars indicate SEM. ***, the punctate fluorescence in the treated sample was significantly lower at $P < 0.0001$. (C) Distribution of the ERAS marker Tip20 before and after auxin-induced degradation of the ERES component Sec23. A strain expressed Tip20-GFP together with OsTIR1 and Sec23-AID. Images were captured before and after treatment with IAA for 30 min. Scale bar, 1 μ m. (D) Quantification of the data from C. The procedure was performed as in B. ***, $P < 0.0001$.

Degradation of Sec26 did not substantially affect the punctate localization of the ERES marker Sec31-mCherry (Fig. 5, D and E), indicating that the disruption of ERAS by COPI inactivation was not an indirect effect of disrupting ERES. We conclude that COPI function is needed to maintain ERAS.

Loss of ERES disrupts Golgi organization

The combined results could be explained if ERES generate Golgi cisternae that bud COPI vesicles to create ERAS. To test this hypothesis, we labeled the early Golgi with GFP-Vig4 and then disrupted ERES by anchoring away the COPII subunits Sec23 and Shl23. After rapamycin addition, the normal pattern of several GFP-Vig4 puncta per cell was converted to a highly fragmented pattern (Fig. 6 A). Thin-section EM confirmed that after ERES were disrupted by rapamycin addition, the tight stacks of Golgi cisternae typically seen in *P. pastoris* cells (Fig. 6 B, -Rapa; Rossanese et al., 1999) were almost completely absent and were replaced by less-organized

membrane structures (Fig. 6 B, + Rapa). Quantification confirmed that the normal stacked organization of the *P. pastoris* Golgi was abolished by anchoring away Sec23 and Shl23 (Fig. 6 C). These data support the idea that loss of ERES disrupts the Golgi compartments that are required for normal ERAS formation.

Loss of ERAS does not disrupt ERES or Golgi organization

The complementary approach was to disrupt ERAS by inactivating Tip20 and to examine the effect on ERES and Golgi structures. First, we used the anchor-away method. To verify that Tip20 could be displaced by this method, we tagged Tip20 simultaneously with FRB and GFP. After addition of rapamycin, the normal punctate ERAS pattern of Tip20 localization was lost (Fig. S6 A). When the experiment was repeated in a strain expressing Tip20-FRB together with the ERES marker Sec31-GFP, anchoring away Tip20 for 10 min did not alter the localization of Sec31 (Fig. 7, A and B). Similar results were seen after 30 min of

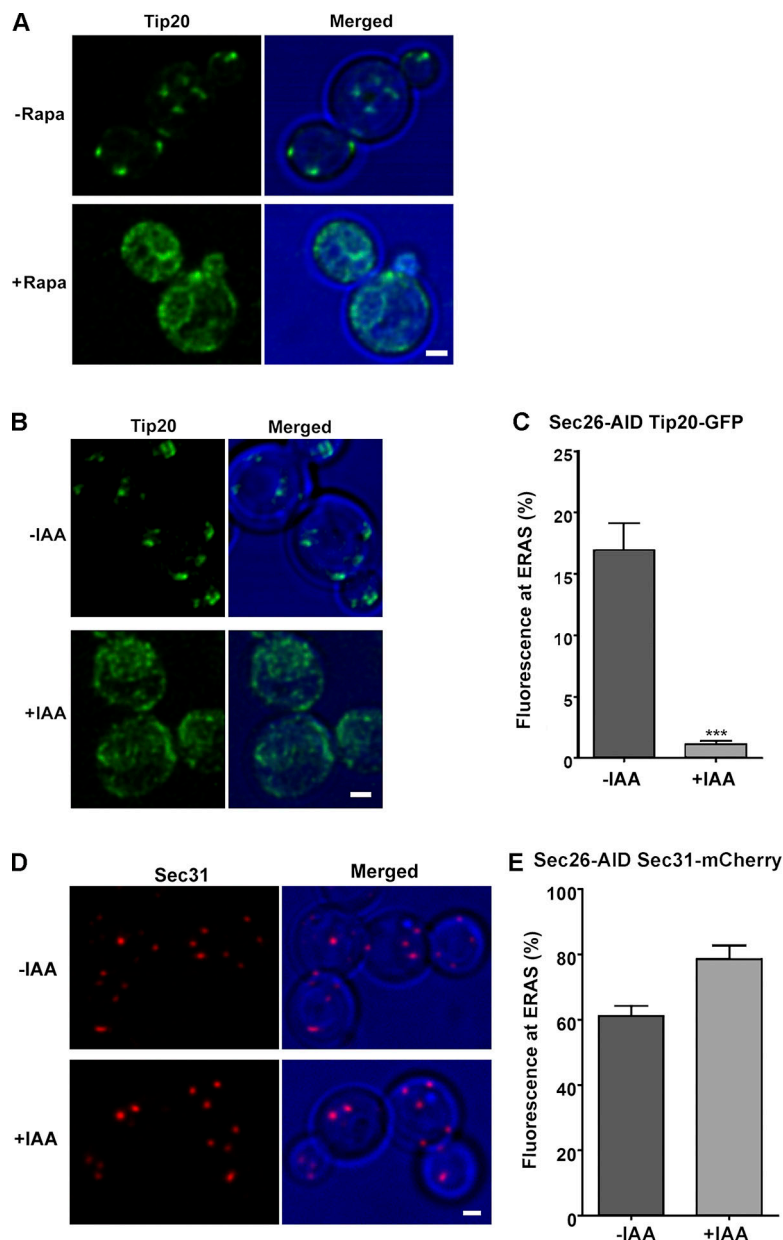


Figure 5. **Effect on ERAS and ERES of inactivating COPI.**

(A) Distribution of the ERAS marker Tip20 before and after anchor-away of the COPI component Sec26. A strain expressed Tip20-GFP together with the Rpl17-FKBPx4 ribosomal anchor as well as Sec26-FRB. Images were captured before and after treatment with rapamycin (Rapa) for 10 min. Scale bar, 1 μ m.

(B) Distribution of the ERAS marker Tip20 before and after auxin-induced degradation of the COPI component Sec26. A strain expressed Tip20-GFP together with OstTIR1 and Sec26-AID. Images were captured before and after treatment with IAA for 30 min. Scale bar, 1 μ m.

(C) Quantification of the data from B. The percentage of the total GFP signal that was present at punctate ERAS was measured for ~20 individual cells in each sample. Bars indicate SEM. ***, the punctate fluorescence in the treated sample was significantly lower at $P < 0.0001$.

(D) Distribution of the ERES marker Sec31 before and after auxin-induced degradation of the COPI component Sec26. A strain expressed Sec31-mCherry together with OstTIR1 and Sec26-AID. Images were captured before and after treatment with IAA for 30 min. Scale bar, 1 μ m.

(E) Quantification of the data from D. The percentage of the total Sec31-mCherry signal that was present at punctate ERES was measured for ~30 individual cells in each sample. Bars indicate SEM.

rapamycin treatment (not depicted). Second, we used the AID system. As a control, Tip20 was degraded in a strain that expressed Dsl3-GFP to mark ERAS. Within 30 min after IAA was added to trigger degradation of Tip20, the punctate Dsl3-GFP labeling became much weaker in most of the cells (Fig. S6, B and C). By contrast, when Tip20 was degraded in a strain that expressed Sec31-GFP to mark ERES, there was no detectable change in the punctate ERES pattern (Fig. 7, C and D). These results suggest that loss of ERAS has little or no effect on ERES organization.

Additional experiments tested the role of ERAS in maintaining Golgi organization. When ERAS were disrupted by anchoring away Tip20, the COPI pattern as marked by Sec26-GFP was not detectably perturbed (Fig. 8, A and B). Similarly, anchoring away Tip20 did not detectably perturb the early Golgi pattern as marked by GFP-Vig4 (Fig. 8, C and D). These results

indicate that ERAS do not play a crucial role in maintaining the structure of ERES-Golgi units in *P. pastoris*.

Putative ERAS are associated with ERES in mammalian cells

P. pastoris is a good model for understanding ERES in mammalian cells (Bevis et al., 2002; Bhattacharyya and Glick, 2007; Montegna et al., 2012; Stephens, 2003), so we asked if the same was true for ERAS. The mammalian counterpart of the Dsl1 complex has been identified (Hirose, 2004; Aoki et al., 2009) and is termed the NRZ complex for the names of its subunits: NAG (counterpart to Dsl3), RINT1 (distantly related Tip20 homologue), and ZW10 (distantly related Dsl1 homologue; Civril et al., 2010; Tagaya et al., 2014). Like the Dsl1 complex, the NRZ complex plays a role in Golgi-to-ER membrane traffic and interacts with ER SNAREs, in this case Syntaxin18 (Ufe1 homologue), BNIP1 (Sec20 homologue), p31 (Use1 homologue), and

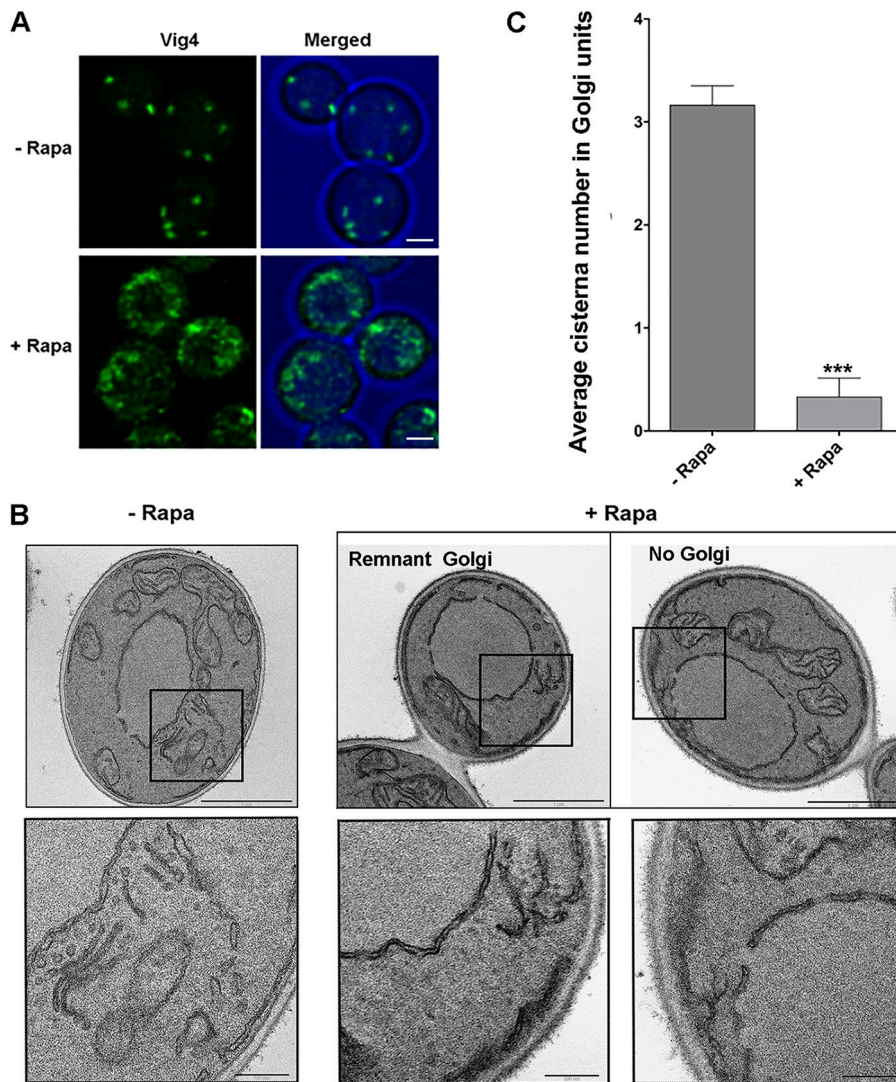


Figure 6. Effect on Golgi structure of disrupting ERES. (A) Distribution of the early Golgi marker Vig4 before and after anchor-away of the ERES components Sec23 and Shl3. A strain expressed GFP-Vig4 together with the Rpl17-FKBPx4 ribosomal anchor as well as Sec23-FRB and Shl23-FRB. Images were captured before and after treatment with rapamycin (Rapa) for 10 min. Scale bar, 1 μ m. (B) Representative thin-section electron micrographs of a strain expressing the Rpl17-FKBPx4 ribosomal anchor as well as Sec23-FRB and Shl23-FRB, showing the loss of tightly stacked Golgi structures after ERES were disrupted by treatment with Rapa for 20 min. Some cells displayed structures that resembled Golgi remnants, and others displayed no recognizable Golgi structures. Scale bars, 1 μ m (top row) or 200 nm (bottom row). (C) Quantification of the EM data from B. The average number of cisternae in tightly stacked Golgi units was measured for ~60 individual cell sections in each sample. Bars indicate SEM. As indicated by the asterisks, the average cisterna number in the rapamycin-treated sample was significantly lower at $P < 0.0001$.

Sec22b (Sec22 homologue; Hatsuzawa et al., 2000; Hirose, 2004; Nakajima, 2004; Aoki et al., 2009; Uemura, 2009). We investigated whether the NRZ complex might mark mammalian ERAS that are associated with ERES. The mammalian ERES marker was Sec16A (Bhattacharyya and Glick, 2007; Watson et al., 2006), and the potential mammalian ERAS marker was RINT1. By immunofluorescence microscopy, RINT1 appeared as punctate structures that consistently showed close association with Sec16A (Fig. 9 A). We also examined Syntaxin 18, which showed only occasional overlap with Sec16A (Fig. 9 B), suggesting that ER-localized SNAREs are not stable components of mammalian ERAS. An in-depth analysis will be needed for mammalian cells, but the result with RINT1 suggests that the mammalian NRZ complex marks ERAS that are associated with ERES.

Discussion

ERES are increasingly well characterized, but the properties and even the existence of ERAS have been less apparent. ERAS can be defined in budding yeasts by the presence of COPI vesicles bound to the Dsl1 complex. However, the *S. cerevisiae* Dsl1

complex is present throughout the ER, and when interactions between COPI and the Dsl1 complex were visualized in *S. cerevisiae*, the results were complex: the putative ERAS were only occasionally associated with ERES and were most often at sites of polarized growth (Schröter et al., 2016). The origin and physiological significance of this pattern are unknown. Our data with *P. pastoris* are clearer, and they indicate that ERAS are associated with ERES. This linkage is strong in that most or all ERES are associated with ERAS and vice versa. Based on the fluorescence microscopy analysis described here, combined with our earlier electron tomography data (Levi et al., 2010; Mogelsvang et al., 2003), we propose that an ERES and its associated ERAS form a bipartite structure. ERAS as visualized with the tagged Dsl1 complex often partially or completely encircle ERES as visualized with tagged COPII. This result suggests that the basic arrangement of an ERES-ERAS unit in *P. pastoris* is a circular area of COPII vesicle-producing ER membrane surrounded by a ring of COPI vesicle-receiving ER membrane (Fig. 10).

How is the architecture of a bipartite ERES-ERAS structure generated? We addressed this question by selectively

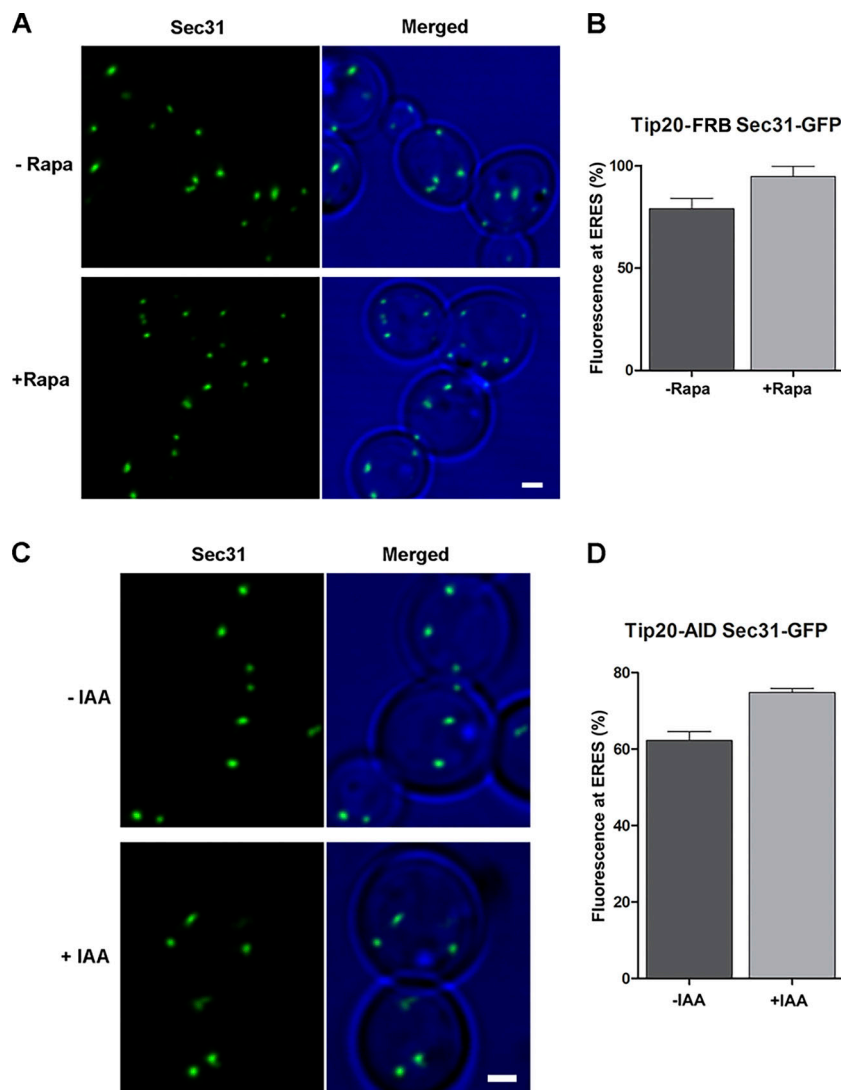


Figure 7. Effect on ERES of disrupting ERAS.

(A) Distribution of the ERES marker Sec31 before and after anchor-away of the ERAS component Tip20. A strain expressed Sec31-GFP together with the Rpl17-FKBPx4 ribosomal anchor as well as Tip20-FRB. Images were captured before and after treatment with rapamycin (Rapa) for 10 min. Scale bar, 1 μ m. **(B)** Quantification of the data from A. The percentage of the total GFP signal that was present at punctate ERES was measured for \sim 20 individual cells in each sample. Bars indicate SEM. **(C)** Distribution of the ERES marker Sec31 before and after auxin-induced degradation of the ERAS component Tip20. A strain expressed Sec31-GFP together with OsTIR1 and Tip20-AID. Images were captured before and after treatment with IAA for 30 min. Scale bar, 1 μ m. **(D)** Quantification of the data from C. The procedure was performed as in B.

inactivating proteins involved in establishing ERES or ERAS. One method was the anchor-away technique, which rapidly inactivates a tagged protein by attaching it to ribosomes (Bharucha et al., 2013; Haruki et al., 2008). A second method employed an AID to degrade a tagged protein (Nishimura et al., 2009; Nishimura and Kanemaki, 2014). The two methods yielded similar results. When ERES were disrupted by inactivating a COPII subunit, ERAS were also disrupted, whereas when ERAS were disrupted by inactivating a Dsl1 complex subunit, ERES were largely unaffected. We infer that ERAS organization relies on the presence of ERES, whereas ERES can persist in the absence of ERAS.

ERAS organization also requires COPI. We find that in *P. pastoris*, COPI often forms partial or complete rings that encircle Golgi proteins such as the GDP-mannose transporter Vig4. This result is reminiscent of evidence that in mammalian cells, membrane traffic proteins are concentrated at the rims of Golgi cisternae while glycosylation enzymes are concentrated in the central portions of the cisternae (Tie et al., 2018). Yet *P. pastoris* COPI also shows strong colocalization with the Dsl1 complex, which is attached to the ER surface. As depicted in Fig. 2 E, we

can reconcile these findings by assuming that the Dsl1 complex links ER proteins to COPI that is present on nascent Golgi-derived vesicles. When scission occurs, the resulting COPI vesicles will already be tethered at ERAS and thus will never diffuse in the cytosol. This guided handover of COPI vesicles to the ER may boost the efficiency of Golgi-to-ER recycling.

According to this view, localization of the Dsl1 complex to discrete ER domains reflects interaction of the Dsl1 complex with Golgi-associated COPI. To test this model, we disrupted Golgi architecture by inactivating ERES. Under those conditions, Golgi cisternae were fragmented and dispersed, presumably because tethering of early Golgi cisternae to the ER was lost (Glick, 2014), and the Dsl1 complex redistributed to the general ER. Our interpretation is that when Golgi structures became fragmented, the ER-associated Dsl1 complex could diffuse laterally, either because the COPI interaction was abolished or because the Dsl1 complex interacted with COPI on Golgi fragments that were no longer held in place.

What links the Dsl1 complex to the ER? An obvious candidate is ER-localized SNAREs that mediate the fusion of retrograde COPI vesicles (Meiringer et al., 2011). We do see some concentration

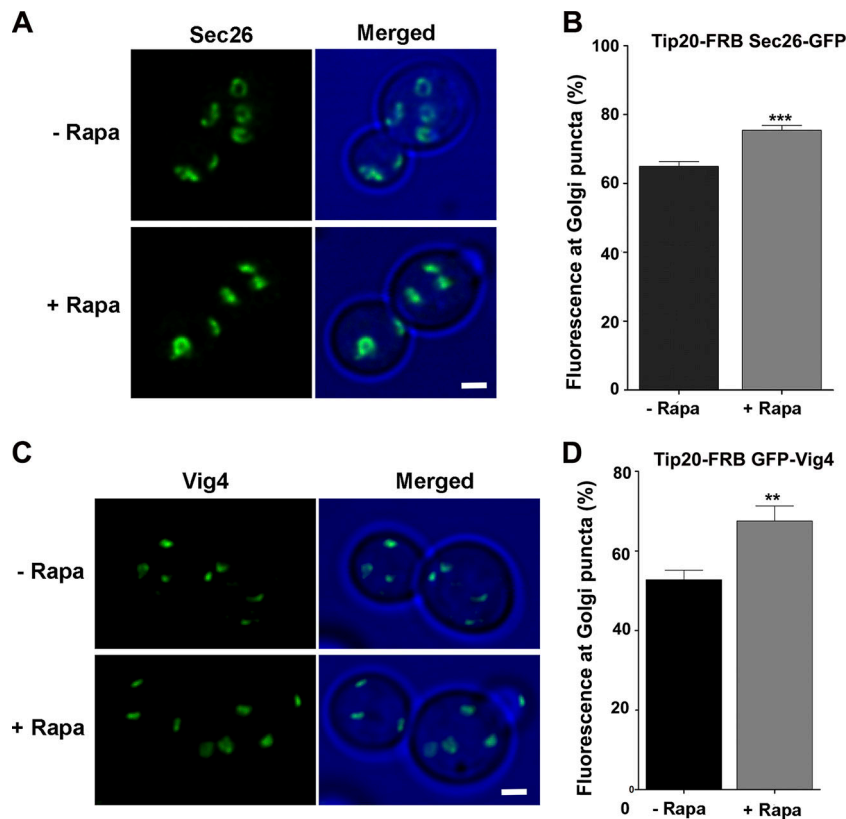


Figure 8. Effect on COPI and the Golgi of disrupting ERAS. (A) Distribution of the COPI maker Sec26 before and after anchor-away of the ERAS component Tip20. The strain expressed Sec26-GFP together with the Rpl17-FKBPx4 ribosomal anchor as well as Tip20-FRB. Images were captured before and after treatment with rapamycin (Rapa) for 30 min. Scale bar, 1 μ m. (B) Quantification of the data from A. The percentage of the total GFP signal that was present at punctate structures was measured for \sim 30 individual cells in each sample. Bars indicate SEM. Asterisks indicate statistical significance at ***, $P < 0.0001$. (C) Distribution of the early Golgi marker Vig4 before and after anchor-away of the ERAS component Tip20. The strain expressed GFP-Vig4 together with the Rpl17-FKBPx4 ribosomal anchor as well as Tip20-FRB. Images were captured before and after treatment with Rapa for 30 min. Scale bar, 1 μ m. (D) Quantification of the data from C. The procedure was performed as in B. Asterisks indicate statistical significance at **, $P < 0.005$.

of ER-localized SNAREs in the vicinity of the Dsl1 complex. However, those signals are relatively weak, suggesting that ER-localized SNAREs are not primarily responsible for localizing the Dsl1 complex to ERAS. Instead, the data suggest that the Dsl1 complex first binds to SNAREs that are diffusing in the general ER, and then binds to Golgi-associated COPI to create functional ERAS.

The combined data suggest a simple model that can explain the formation of ERAS and their relationship to ERES. We propose that ERES generate early Golgi cisternae in a process that requires COPII. These early Golgi cisternae recruit COPI at their rims. Meanwhile, ER-localized SNAREs recruit the Dsl1 complex. Then the ER-associated Dsl1 complex binds to Golgi-associated COPI, forming ring-like structures that function as ERAS. The resulting ERES-ERAS pairs serve as bidirectional portals that mediate efficient local traffic between the ER and the Golgi. Validation of this model will require functional evidence that retrograde COPI vesicles fuse with the ER at the putative ERAS.

The mammalian NRZ complex is analogous to the yeast Dsl1 complex, and we find that RINT1, the Tip20 homologue in the NRZ complex, is present in punctate structures associated with ERES. This observation suggests the exciting possibility that ERAS of the type seen in *P. pastoris* are broadly conserved. RINT1 was recently shown to be functionally associated with ERES that are involved in collagen export (Raote et al., 2018). More generally, the ERAS-ERAS relationship may be elaborated in cells that export large and complex cargoes from the ER (Peotter et al., 2019; Raote and Malhotra, 2019). In mammalian cells, retrograde COPI vesicles bud from ERGIC elements (Appenzeller-Herzog and Hauri, 2006; Hammond and Glick, 2000), which

likely play a role in ERAS formation analogous to the role played by early Golgi cisternae in *P. pastoris*. We suggest that in organisms ranging from yeast to mammals, the first functional element in the secretory pathway is a set of linked ERES-ERAS structures that act as bidirectional portals at the ER-Golgi interface.

Materials and methods

General yeast manipulation and molecular biology methods

All experiments were performed with derivatives of the haploid *P. pastoris* strain PPY12 (*his4 arg4*; Gould et al., 1992; Table S1 and Table S2). The cells were transformed with linearized integrating vectors using electroporation. Cultures were grown in rich glucose medium (yeast extract, peptone, dextrose), synthetic glucose medium (SD), or nonfluorescent synthetic glucose medium (NSD; Bevis et al., 2002) in baffled flasks at 30°C with shaking at 200 rpm. *P. pastoris* gene sequences were obtained from the NCBI database. Molecular biology procedures were simulated and recorded using SnapGene software. The plasmids used in this study are listed in Table S1.

Functional inactivation of proteins with the anchor-away method

A PPY12 derivative suitable for anchor-away experiments was constructed as described previously (Bharucha et al., 2013). In brief, the *TOR1* gene was modified to confer rapamycin resistance, the *FPRI* gene was deleted, and the ribosomal protein Rpl17 was C-terminally tagged with FKBPx4. The protein to be inactivated was tagged with FRB by gene replacement. Yeast cells grown to midlog phase were treated with 1 μ g/ml rapamycin

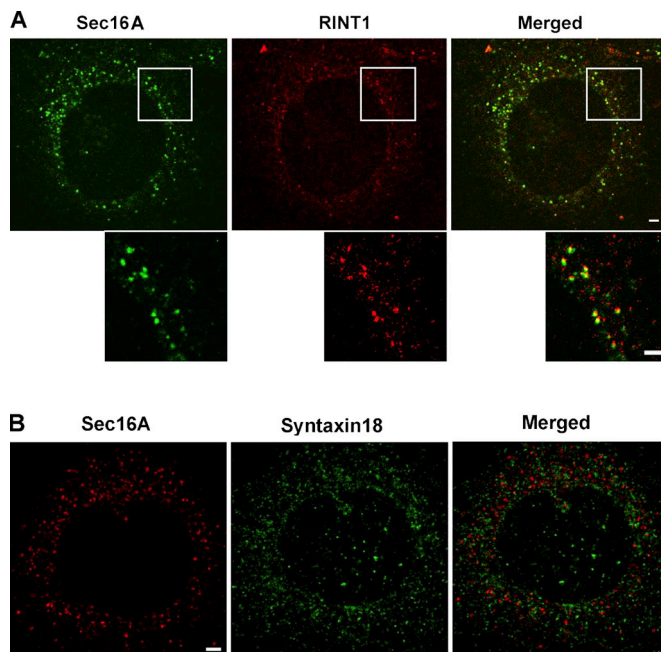


Figure 9. **Putative ERAS in cultured human U2OS cells.** (A) Consistent close association of the Tip20 homologue RINT1 with the ERES marker Sec16A. Immunofluorescence microscopy was used to visualize Sec16A together with RINT1, a subunit of the NRZ complex. The insets are magnified twofold relative to the original images. Scale bars, 5 μm . (B) Lack of consistent association of the Ufe1 homologue Syntaxin18 with the ERES marker Sec16A. Immunofluorescence microscopy was used to visualize Sec16A together with Syntaxin18, an ER-localized SNARE. Scale bar, 5 μm .

added from a 1 mg/ml stock in 90% ethanol/10% Tween 20, and were imaged after \sim 10 min.

Depletion of proteins using an AID

Plasmids containing the 3x-mini-AID cassette (Kubota et al., 2013) and a yeast codon-optimized version of the plant *OstTIRI* gene were provided by the National Bio Resource Project–Yeast (Kyoto, Japan). The *OstTIRI* gene was amplified by PCR from plasmid BYP7569 using primers 5'-GATCGGCATGCTCATAAAATCTTGACGAAGTTAGGAGCATC-3' and 5'-GATCGGGTACCAAATGACTTATTTTCCTGAAGAAGTTGTAGAACAC-3', digested with KpnI and SphI, and subcloned into the constitutive expression vector pIB2 (Sears et al., 1998) cut with the same enzymes. This construct was linearized with SalI for integration at the *HIS4* locus. The protein to be degraded was then tagged with 3x-mini-AID by gene replacement. Yeast cells grown to midlog phase were treated with 1 mM IAA and were imaged after \sim 30 min.

Construction of strains expressing tagged Tip20

A 3' portion of the *P. pastoris* *TIP20* coding sequence plus a downstream region were amplified by PCR, and this fragment was inserted between the EcoRI and PstI sites of pUC19-ARG4 (Rossanese et al., 1999). BamHI and NotI sites were introduced by site-directed mutagenesis in place of the stop codon. 3xGFP, 3xmCherry, 3x-mini-AID, and FRB cassettes excised with BamHI and NotI were inserted. The GFP variant used was iGFP (Day

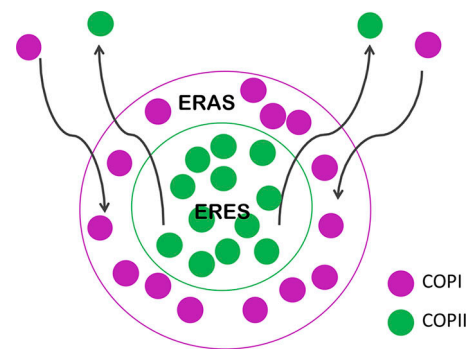


Figure 10. **Model for the relationship between ERES and ERAS.** We propose that in *P. pastoris* and likely also in other organisms, each ERES is surrounded by a ring-like ERAS that depends on the ERES for its integrity.

et al., 2018). These plasmids were linearized with BspEI and integrated at the *TIP20* locus. Additional plasmids were generated to use the constructs in Arg⁺ strains, as follows. Tip20-3xGFP was amplified by PCR and subcloned into pAG32 (Goldstein and McCusker, 1999) between the SacI and SpeI sites. This plasmid was linearized with EcoRV for integration, followed by selection with hygromycin B. Tip20-3xmCherry was excised with EcoRI and SphI and subcloned into pUC19-kanMX (Montegna et al., 2012) cut with the same enzymes. This plasmid was linearized with EcoRV for integration, followed by selection with G418.

Construction of strains expressing tagged Dsl3

A 3' portion of the *P. pastoris* *DSL3* coding sequence plus a downstream region were amplified by PCR, and this fragment was inserted between the KpnI and SphI sites of pUC19-ARG4. BamHI and NotI sites were introduced by site-directed mutagenesis in place of the stop codon. 3xGFP and 3xmCherry cassettes excised with BamHI and NotI were inserted. These plasmids were linearized with XbaI and integrated at the *DSL3* locus. Additional plasmids were generated to use the constructs in Arg⁺ strains, as follows. Dsl3-3xGFP was amplified by PCR and subcloned into pUG6 (Guldener et al., 1996) between the XhoI and SpeI sites. This plasmid was linearized with EcoRI for integration, followed by selection with G418. Dsl3-3xmCherry was excised with KpnI and SphI and subcloned into pUC19-HIS4 (Connerly et al., 2005). This plasmid was transformed into a dam⁻ *Escherichia coli* strain and then linearized with BclI for integration at the *HIS4* locus.

Construction of strains expressing tagged Sec23

A 3' portion of the *P. pastoris* *SEC23* coding sequence (Esaki et al., 2006) plus a downstream region were amplified by PCR, and this fragment was inserted between the EcoRI and SphI sites of pUC19-ARG4. BamHI and NotI sites were introduced by site-directed mutagenesis in place of the stop codon. A 3x-mini-AID cassette excised with BamHI and NotI was inserted. This plasmid was linearized with NsiI and integrated at the *SEC23* locus.

Construction of strains expressing tagged Sec31

A pAG32 derivative expressing Sec31-msGFP (Bharucha et al., 2013) was linearized with EcoNI and integrated at the *SEC31*

locus. To swap the drug resistance marker, the Sec31-GFP fragment was excised with NdeI and XbaI and subcloned into pUG6 cut with the same enzymes. This plasmid was linearized with AccI and integrated at the *SEC31* locus.

Construction of strains expressing tagged Sec13

A plasmid for expression of Sec13-EGFP (Rossanese et al., 1999) was modified by replacing EGFP with msGFP (Fitzgerald and Glick, 2014). The resulting plasmid was further modified by replacing msGFP with a yeast codon-optimized HaloTag (Day et al., 2018) using the NcoI and EagI sites. The Sec13-msGFP plasmid, and a similar plasmid for expression of Sec13-DsRed (Connerly et al., 2005), were linearized with MscI and integrated at the *SEC13* locus. The Sec13-HaloTag plasmid was linearized by PCR amplification and integrated at the *SEC13* locus, and the fused gene was verified by PCR amplification from the genomic DNA followed by sequencing.

Construction of strains expressing tagged Sec26

A 3' portion of the *P. pastoris* *SEC26* coding sequence plus a downstream region were amplified by PCR, and this fragment was inserted between the Ecl136II and PstI sites of pUC19-HIS4 (Connerly et al., 2005). BamHI and NotI sites were introduced by site-directed mutagenesis in place of the stop codon. Cassettes encoding msGFP, 3x-mini-AID, FRB, or 3xmCherry were excised with BamHI and NotI and inserted. These plasmids were linearized with KpnI and integrated at the *SEC26* locus.

Construction of a DsRed-HDEL strain

pIB2-DsRed-HDEL (Bevis et al., 2002) was linearized with SalI and integrated at the *HIS4* locus.

Construction of a strain expressing tagged Vig4

The full-length *P. pastoris* *VIG4* gene was amplified by PCR. This fragment was digested with EcoRI and SphI and subcloned into pIB1 (Sears et al., 1998) cut with the same enzymes. BamHI and NotI sites were introduced by site-directed mutagenesis immediately after the start codon, and a cassette encoding msGFP was excised with BamHI and NotI and inserted (Jain et al., 2019). This plasmid was linearized with StuI and integrated at the *HIS4* locus.

Construction of a strain expressing tagged Sec7

A pUC19-ARG4 derivative containing a 3' portion of the *P. pastoris* *SEC7* coding sequence plus a downstream region (Bevis et al., 2002) was modified by inserting a 6xDsRed.M1 cassette in place of the stop codon (Losev et al., 2006). This plasmid was linearized with XmnI and integrated at the *SEC7* locus (Jain et al., 2018; Jain et al., 2019).

Construction of a strain expressing tagged Sec20

The full-length *P. pastoris* *SEC20* gene was amplified by PCR. This fragment was digested with EcoRI and HindIII and subcloned into pUC19-ARG4 cut with the same enzymes. BamHI and NotI sites were introduced by site-directed mutagenesis immediately after the start codon, and a cassette encoding iGFP was excised with BamHI and NotI and inserted. This plasmid was linearized with XbaI and integrated at the *SEC20* locus.

Construction of a strain expressing tagged Sec63

A 3' portion of the *P. pastoris* *SEC63* coding sequence plus a downstream region were amplified by PCR, and this fragment was inserted between the EcoRI and HindIII sites of pUC19-ARG4. BamHI and NotI sites were introduced by site-directed mutagenesis in place of the stop codon. A 3xmCherry cassette excised with BamHI and NotI was inserted. This plasmid was linearized with EcoNI and integrated at the *SEC63* locus.

Fluorescence microscopy of yeast

Confocal imaging of live cells was performed with a Leica SP8 using a 100× 1.4-NA objective. Cells were grown to log phase in SD or NSD, immobilized on glass-bottom dishes using concanavalin A, washed, covered with SD or NSD, and imaged at 30°C (Day et al., 2016). One- or two-color datasets were obtained using separate excitation and capture of red and green signals, with a pinhole of 1.2 a.u. and with a line averaging of 8. We used a pixel size of 60–70 nm, a frame size of 256 × 128 or 256 × 256 pixels, and a Z-step interval of 0.30 μm. For 4D imaging, Z-stacks were collected at intervals of 2 s. Three-color imaging using the JF₆₄₆ HaloTag dye (Grimm et al., 2015) was performed as previously described (Casler et al., 2019). The image stacks were deconvolved using Huygens Professional software and further processed using ImageJ (National Institutes of Health; Schneider et al., 2012). Average projected fluorescence micrographs were assembled using Adobe Photoshop. Micrographs labeled “merged” include transmitted light images of the cells.

Quantification of fluorescence data

For static images, the overlap between two punctate fluorescence signals was quantified as previously described (Levi et al., 2010), and the percentage of a fluorescent signal present in punctate structures was quantified as previously described (Bharucha et al., 2013). For 4D videos, quantification of fluorescence signals was performed using custom ImageJ plugins (Day et al., 2016) as follows. Deconvolved image sequence stacks were bleach-corrected for each channel and converted into 4D montage series, which were further converted to 8-bit hyperstacks. A plugin was used to calculate the fluorescence over time for individual punctate structures. All quantification data were plotted using GraphPad Prism software. The statistical significance of differences between pairs of samples was determined by a paired two-tailed Student's *t* test.

Immunofluorescence microscopy of mammalian cells

For immunofluorescence, U2OS cells were seeded on glass coverslips and then imaged as previously described (Bhattacharyya et al., 2010). The anti-Sec16A antibody was from Bethyl Laboratories (product no. A300-648A), and the anti-RINT1 and anti-Syntaxin18 antibodies were from Santa Cruz Biotechnology (product nos. sc-19404 and sc-293067). For double labeling of Sec16A and RINT1, the secondary antibodies from Thermo Fisher Scientific were Alexa Fluor 488-conjugated chicken anti-rabbit IgG (product no. A-21441) and Alexa Fluor 568-conjugated rabbit anti-goat IgG (product no. A-11079). For double labeling of Sec16A and Syntaxin18, the secondary antibodies from Thermo Fisher Scientific were Alexa Fluor 594-conjugated chicken

anti-rabbit IgG (product no. A-21442) and Alexa Fluor 488-conjugated donkey anti-mouse IgG (product no. A-21202). Primary antibodies were diluted 1:100, and secondary antibodies were diluted 1:200. Mounted samples were imaged as confocal Z-stacks using a Leica SP8 microscope with a 63× 1.4-NA objective and a zoom factor of 2.

EM

EM of *P. pastoris* cells was performed as previously described (Levi et al., 2010). Briefly, a 50-ml culture of yeast cells was grown in rich glucose medium to an OD₆₀₀ of ~0.5. The culture was concentrated to a volume of <5 ml with a bottle-top vacuum filter and was fixed by adding 40 ml of ice-cold 50 mM KPi, pH 6.8, 1 mM MgCl₂, and 2% glutaraldehyde and leaving on ice for 1 h. The cells were washed repeatedly and then resuspended in 0.75 ml of 4% KMnO₄ and mixed for 1 h at room temperature. The cells were washed, resuspended in 0.75 ml of 2% uranyl acetate, and mixed for 1 h at room temperature. Finally, the cells were washed and dehydrated and embedded in Spurr's resin. The resin was polymerized for 2 d at 68°C. Thin sections were stained with uranyl acetate and lead citrate and were viewed with a JEOL 100CX II electron microscope.

Online supplemental material

Fig. S1 shows that Dsl1 complex subunits colocalize with COPI and are closely associated with early and late Golgi markers. Fig. S2 extends the localization analysis to include the Dsl3 subunit of the Dsl1 complex as well as ER-localized SNAREs. Figs. S3 and S4 use different ERAS markers to study the de novo formation and fusion of ERAS in association with ERES. Fig. S5 shows the effects of Sec23 degradation on ERES and ERAS. Fig. S6 shows control experiments to document that Tip20 is efficiently inactivated by either the anchor-away method or auxin-induced degradation. Video 1 shows coupled de novo formation of ERES and ERAS. Video 2 shows coupled fusion of ERES and ERAS. Video 3 shows that the coupled dynamics of ERES and ERAS are unchanged when the fluorescent tags are swapped. Videos 4 and 5 show that when alternative markers are used, ERES and ERAS still show coupled de novo formation and fusion, respectively. Table S1 shows plasmid constructs used in this study, and Table S2 shows *P. pastoris* strains used in this study.

Acknowledgments

We thank Sophie Travis and Fred Hughson for helpful discussion about the structure of the Dsl1-SNARE complex and Luke Lavis for generously providing the JF₆₄₆ dye.

This study was supported by Department of Biotechnology, Ministry of Science and Technology grant 102/IFD/SAN/2282/2012-2013 to D. Bhattacharyya. C. Bhattacharjee was supported by University Grants Commission postdoctoral grant F.15-1/2013-14/PDFWM-2013-14-GE-MEG-21765(SAII), and S. Roy Chowdhury and B.K. Jain were supported by Homi Bhabha National Institute pre-doctoral fellowships. B.S. Glick was supported by National Institutes of Health grant R01 GM104010, and J.C. Casler was supported by National Institutes of Health training grant T32 GM007183.

The authors declare no competing financial interests.

Author contributions: S. Roy Chowdhury performed the majority of the experiments, created most of the constructs and strains, performed the final microscopy analysis, and drafted the figures. C. Bhattacharjee initiated the project, carried out the initial standardizations, experiments, and analysis, performed the mammalian immunofluorescence experiments, and helped to draft the figures. J.C. Casler generated vector for auxin-inducible degradation, showed that anchor-away of Sec26 disrupts Tip20 localization, and performed three-color imaging. B.K. Jain constructed the Sec7 and Vig4 plasmids and assisted in quantitative analysis. B.S. Glick provided input about the experimental analysis and helped to revise the manuscript. D. Bhattacharyya supervised the project, and prepared the manuscript and figures.

Submitted: 18 February 2019

Revised: 11 July 2019

Accepted: 17 January 2020

References

- Aoki, T., S. Ichimura, A. Itoh, M. Kuramoto, T. Shinkawa, T. Isobe, and M. Tagaya. 2009. Identification of the neuroblastoma-amplified gene product as a component of the syntaxin 18 complex implicated in Golgi-to-endoplasmic reticulum retrograde transport. *Mol Biol Cell*. 20: 2639–2649. <https://doi.org/10.1091/mbc.e08-11-1104>
- Appenzeller-Herzog, C., and H.P. Hauri. 2006. The ER-Golgi intermediate compartment (ERGIC): in search of its identity and function. *J. Cell Sci*. 119:2173–2183. <https://doi.org/10.1242/jcs.03019>
- Arakawa, K., M. Abe, Y. Noda, H. Adachi, and K. Yoda. 2006. Molecular cloning and characterization of a *Pichia pastoris* ortholog of the yeast Golgi GDP-mannose transporter gene. *J. Gen. Appl. Microbiol.* 52:137–145. <https://doi.org/10.2323/jgam.52.137>
- Bevis, B.J., A.T. Hammond, C.A. Reinke, and B.S. Glick. 2002. De novo formation of transitional ER sites and Golgi structures in *Pichia pastoris*. *Nat. Cell Biol.* 4:750–756. <https://doi.org/10.1038/ncb852>
- Bharucha, N., Y. Liu, E. Papanikou, C. McMahon, M. Esaki, P.D. Jeffrey, F.M. Hughson, and B.S. Glick. 2013. Sec16 influences transitional ER sites by regulating rather than organizing COPII. *Mol. Biol. Cell*. 24:3406–3419. <https://doi.org/10.1091/mbc.e13-04-0185>
- Bhattacharyya, D., and B.S. Glick. 2007. Two mammalian Sec16 homologues have nonredundant functions in endoplasmic reticulum (ER) export and transitional ER organization. *Mol. Biol. Cell*. 18:839–849. <https://doi.org/10.1091/mbc.e06-08-0707>
- Bhattacharyya, D., A.T. Hammond, and B.S. Glick. 2010. High-quality immunofluorescence of cultured cells. *Methods Mol. Biol.* 619:403–410. https://doi.org/10.1007/978-1-60327-412-8_24
- Budnik, A., and D.J. Stephens. 2009. ER exit sites—localization and control of COPII vesicle formation. *FEBS Lett.* 583:3796–3803. <https://doi.org/10.1016/j.febslet.2009.10.038>
- Casler, J.C., E. Papanikou, J.J. Barrero, and B.S. Glick. 2019. Maturation-driven transport and AP-1-dependent recycling of a secretory cargo in the Golgi. *J. Cell Biol.* 218:1582–1601. <https://doi.org/10.1083/jcb.201807195>
- Civril, F., A. Wehenkel, F.M. Giorgi, S. Santaguida, A. Di Fonzo, G. Grigorean, F.D. Ciccarelli, and A. Musacchio. 2010. Structural analysis of the RZZ complex reveals common ancestry with multisubunit vesicle tethering machinery. *Structure*. 18:616–626. <https://doi.org/10.1016/j.str.2010.02.014>
- Connerly, P.L., M. Esaki, E.A. Montegna, D.E. Strongin, S. Levi, J. Soderholm, and B.S. Glick. 2005. Sec16 is a determinant of transitional ER organization. *Curr. Biol.* 15:1439–1447. <https://doi.org/10.1016/j.cub.2005.06.065>
- Cosson, P., and F. Letourneur. 1997. Coatamer (COPI)-coated vesicles: role in intracellular transport and protein sorting. *Curr. Opin. Cell Biol.* 9: 484–487. [https://doi.org/10.1016/S0955-0674\(97\)80023-3](https://doi.org/10.1016/S0955-0674(97)80023-3)
- Day, K.J., J.C. Casler, and B.S. Glick. 2018. Budding yeast has a minimal endomembrane system. *Dev. Cell.* 44:56–72.e4. <https://doi.org/10.1016/j.devcel.2017.12.014>

- Day, K.J., E. Papanikou, and B.S. Glick. 2016. 4D confocal imaging of yeast organelles. *Methods Mol. Biol.* 1496:1–11. https://doi.org/10.1007/978-1-4939-6463-5_1
- Duden, R., M. Hosobuchi, S. Hamamoto, M. Winey, B. Byers, and R. Schekman. 1994. Yeast β - and β' -coat proteins (COP). Two coatomer subunits essential for endoplasmic reticulum-to-Golgi protein traffic. *J. Biol. Chem.* 269:24486–24495.
- Esaki, M., Y. Liu, and B.S. Glick. 2006. The budding yeast *Pichia pastoris* has a novel Sec23p homolog. *FEBS Lett.* 580:5215–5221. <https://doi.org/10.1016/j.febslet.2006.08.058>
- Fitzgerald, I., and B.S. Glick. 2014. Secretion of a foreign protein from budding yeasts is enhanced by cotranslational translocation and by suppression of vacuolar targeting. *Microb. Cell Fact.* 13:125. <https://doi.org/10.1186/s12934-014-0125-0>
- Glick, B.S. 2014. Integrated self-organization of transitional ER and early Golgi compartments. *BioEssays.* 36:129–133. <https://doi.org/10.1002/bies.201300131>
- Goldstein, A.L., and J.H. McCusker. 1999. Three new dominant drug resistance cassettes for gene disruption in *Saccharomyces cerevisiae*. *Yeast.* 15: 1541–1553. [https://doi.org/10.1002/\(SICI\)1097-0061\(199910\)15:14<1541::AID-YEA476>3.0.CO;2-K](https://doi.org/10.1002/(SICI)1097-0061(199910)15:14<1541::AID-YEA476>3.0.CO;2-K)
- Gould, S.J., D. McCollum, A.P. Spong, J.A. Heyman, and S. Subramani. 1992. Development of the yeast *Pichia pastoris* as a model organism for a genetic and molecular analysis of peroxisome assembly. *Yeast.* 8:613–628. <https://doi.org/10.1002/yea.320080805>
- Grimm, J.B., B.P. English, J. Chen, J.P. Slaughter, Z. Zhang, A. Revyakin, R. Patel, J.J. Macklin, D. Normanno, R.H. Singer, et al. 2015. A general method to improve fluorophores for live-cell and single-molecule microscopy. *Nat. Methods.* 12:244–250. <https://doi.org/10.1038/nmeth.3256>
- Güldener, U., S. Heck, T. Fielder, J. Beinhauer, and J.H. Hegemann. 1996. A new efficient gene disruption cassette for repeated use in budding yeast. *Nucleic Acids Res.* 24:2519–2524. <https://doi.org/10.1093/nar/24.13.2519>
- Hammond, A.T., and B.S. Glick. 2000. Dynamics of transitional endoplasmic reticulum sites in vertebrate cells. *Mol. Biol. Cell.* 11:3013–3030. <https://doi.org/10.1091/mbc.11.9.3013>
- Haruki, H., J. Nishikawa, and U.K. Laemmli. 2008. The anchor-away technique: rapid, conditional establishment of yeast mutant phenotypes. *Mol. Cell.* 31:925–932. <https://doi.org/10.1016/j.molcel.2008.07.020>
- Jain, B.K., R. Dahara, and D. Bhattacharyya. 2019. The golgin Pplmh1 mediates reversible cisternal stacking in the Golgi of the budding yeast *Pichia pastoris*. *J. Cell Sci.* 132:jcs230672. <https://doi.org/10.1242/jcs.230672>
- Hatsuzawa, K., H. Hirose, K. Tani, A. Yamamoto, R.H. Scheller, and M. Tagaya. 2000. Syntaxin 18, a SNAP receptor that functions in the endoplasmic reticulum, intermediate compartment, and cis-Golgi vesicle trafficking. *J Biol Chem.* 275:13713–13720. <https://doi.org/10.1074/jbc.275.18.13713>
- Hirose, H., et al. 2004. Implication of ZW10 in membrane trafficking between the endoplasmic reticulum and Golgi. *EMBO J.* 23:1267–1278. <https://doi.org/10.1038/sj.emboj.7600135>
- Jain, B.K., P.S. Thapa, A. Varma, and D. Bhattacharyya. 2018. Identification and characterization of GRIP domain Golgin Pplmh1 from *Pichia pastoris*. *Yeast.* 35:499–506. <https://doi.org/10.1002/yea.3317>
- Kraynack, B.A., et al. 2005. Dsl1p, Tip20p, and the novel Dsl3(Sec39) protein are required for the stability of the Q/t-SNARE complex at the endoplasmic reticulum in yeast. *Mol Biol Cell.* 16:3963–3977. <https://doi.org/10.1091/mbc.e05-01-0056>
- Kubota, T., K. Nishimura, M.T. Kanemaki, and A.D. Donaldson. 2013. The Elg1 replication factor C-like complex functions in PCNA unloading during DNA replication. *Mol. Cell.* 50:273–280. <https://doi.org/10.1016/j.molcel.2013.02.012>
- Langhans, M., T. Meckel, A. Kress, A. Lerich, and D.G. Robinson. 2012. ERES (ER exit sites) and the “secretory unit concept”. *J. Microsc.* 247:48–59. <https://doi.org/10.1111/j.1365-2818.2011.03597.x>
- Lerich, A., S. Hillmer, M. Langhans, D. Scheuring, P. van Bentum, and D.G. Robinson. 2012. ER import sites and their relationship to ER exit sites: a new model for bidirectional ER-Golgi transport in higher plants. *Front. Plant Sci.* 3:143. <https://doi.org/10.3389/fpls.2012.00143>
- Levi, S.K., D. Bhattacharyya, R.L. Strack, J.R. Austin II, and B.S. Glick. 2010. The yeast GRASP Grh1 colocalizes with COPII and is dispensable for organizing the secretory pathway. *Traffic.* 11:1168–1179. <https://doi.org/10.1111/j.1600-0854.2010.01089.x>
- Losev, E., C.A. Reinke, J. Jellen, D.E. Strongin, B.J. Bevis, and B.S. Glick. 2006. Golgi maturation visualized in living yeast. *Nature.* 441:1002–1006. <https://doi.org/10.1038/nature04717>
- Mardones, G.A., C.M. Snyder, and K.E. Howell. 2006. Cis-Golgi matrix proteins move directly to endoplasmic reticulum exit sites by association with tubules. *Mol. Biol. Cell.* 17:525–538. <https://doi.org/10.1091/mbc.e05-05-0447>
- Marsh, B.J., D.N. Mastrorarde, J.R. McIntosh, and K.E. Howell. 2001. Structural evidence for multiple transport mechanisms through the Golgi in the pancreatic beta-cell line, HIT-T15. *Biochem. Soc. Trans.* 29:461–467. <https://doi.org/10.1042/bst0290461>
- Meiringer, C.T., R. Rethmeier, K. Auffarth, J. Wilson, A. Perz, C. Barlowe, H.D. Schmitt, and C. Ungermann. 2011. The Dsl1 protein tethering complex is a resident endoplasmic reticulum complex, which interacts with five soluble NSF (N-ethylmaleimide-sensitive factor) attachment protein receptors (SNAREs): implications for fusion and fusion regulation. *J. Biol. Chem.* 286:25039–25046. <https://doi.org/10.1074/jbc.M110.215327>
- Michelsen, K., V. Schmid, J. Metz, K. Heusser, U. Liebel, T. Schwede, A. Spang, and B. Schwappach. 2007. Novel cargo-binding site in the beta and delta subunits of coatomer. *J. Cell Biol.* 179:209–217. <https://doi.org/10.1083/jcb.200704142>
- Miller, E.A., and C. Barlowe. 2010. Regulation of coat assembly--sorting things out at the ER. *Curr. Opin. Cell Biol.* 22:447–453. <https://doi.org/10.1016/j.ceb.2010.04.003>
- Mogelsvang, S., N. Gomez-Ospina, J. Soderholm, B.S. Glick, and L.A. Staehelin. 2003. Tomographic evidence for continuous turnover of Golgi cisternae in *Pichia pastoris*. *Mol. Biol. Cell.* 14:2277–2291. <https://doi.org/10.1091/mbc.e02-10-0697>
- Montegna, E.A., M. Bhawe, Y. Liu, D. Bhattacharyya, and B.S. Glick. 2012. Sec12 binds to Sec16 at transitional ER sites. *PLoS One.* 7:e31156. <https://doi.org/10.1371/journal.pone.0031156>
- Nakajima, K.H., et al. 2004. Involvement of BNIPI in apoptosis and endoplasmic reticulum membrane fusion. *EMBO J.* 23:3216–3226. <https://doi.org/10.1038/sj.emboj.7600333>
- Nishimura, K., and M.T. Kanemaki. 2014. Rapid depletion of budding yeast proteins via the fusion of an auxin-inducible degron (AID). *Curr. Protoc. Cell Biol.* 64:20.29.21–20.29.16.
- Nishimura, K., T. Fukagawa, H. Takisawa, T. Takimoto, and M. Kanemaki. 2009. An auxin-based degron system for the rapid depletion of proteins in non-plant cells. *Nat. Methods.* 6:917–922. <https://doi.org/10.1038/nmeth.1401>
- Orci, L., M. Stammes, M. Ravazzola, M. Amherdt, A. Perrelet, T.H. Söllner, and J.E. Rothman. 1997. Bidirectional transport by distinct populations of COPI-coated vesicles. *Cell.* 90:335–349. [https://doi.org/10.1016/S0092-8674\(00\)80341-4](https://doi.org/10.1016/S0092-8674(00)80341-4)
- Peotter, J., W. Kasberg, I. Pustova, and A. Audhya. 2019. COPII-mediated trafficking at the ER/ERGIC interface. *Traffic.* 20:491–503. <https://doi.org/10.1111/tra.12654>
- Raote, I., and V. Malhotra. 2019. Protein transport by vesicles and tunnels. *J. Cell Biol.* 218:737–739. <https://doi.org/10.1083/jcb.201811073>
- Raote, I., M. Ortega-Bellido, A.J. Santos, O. Foresti, C. Zhang, M.F. Garcia-Parajo, F. Campelo, and V. Malhotra. 2018. TANGO1 builds a machine for collagen export by recruiting and spatially organizing COPII, tethers and membranes. *eLife.* 7:e32723. <https://doi.org/10.7554/eLife.32723>
- Ren, Y., C.K. Yip, A. Tripathi, D. Huie, P.D. Jeffrey, T. Walz, and F.M. Hughson. 2009. A structure-based mechanism for vesicle capture by the multisubunit tethering complex Dsl1. *Cell.* 139:1119–1129. <https://doi.org/10.1016/j.cell.2009.11.002>
- Rossanese, O.W., J. Soderholm, B.J. Bevis, I.B. Sears, J. O'Connor, E.K. Williamson, and B.S. Glick. 1999. Golgi structure correlates with transitional endoplasmic reticulum organization in *Pichia pastoris* and *Saccharomyces cerevisiae*. *J. Cell Biol.* 145:69–81. <https://doi.org/10.1083/jcb.145.1.69>
- Sato, K., M. Sato, and A. Nakano. 2001. Rer1p, a retrieval receptor for endoplasmic reticulum membrane proteins, is dynamically localized to the Golgi apparatus by coatomer. *J. Cell Biol.* 152:935–944. <https://doi.org/10.1083/jcb.152.5.935>
- Schneider, C.A., W.S. Rasband, and K.W. Eliceiri. 2012. NIH Image to ImageJ: 25 years of image analysis. *Nat. Methods.* 9:671–675. <https://doi.org/10.1038/nmeth.2089>
- Schröter, S., S. Beckmann, and H.D. Schmitt. 2016. ER arrival sites for COPI vesicles localize to hotspots of membrane trafficking. *EMBO J.* 35: 1935–1955. <https://doi.org/10.15252/emboj.201592873>
- Sears, I.B., J. O'Connor, O.W. Rossanese, and B.S. Glick. 1998. A versatile set of vectors for constitutive and regulated gene expression in *Pichia pastoris*. *Yeast.* 14:783–790. [https://doi.org/10.1002/\(SICI\)1097-0061\(19980615\)14:8<783::AID-YEA272>3.0.CO;2-Y](https://doi.org/10.1002/(SICI)1097-0061(19980615)14:8<783::AID-YEA272>3.0.CO;2-Y)
- Spang, A. 2009. On vesicle formation and tethering in the ER-Golgi shuttle. *Curr. Opin. Cell Biol.* 21:531–536. <https://doi.org/10.1016/j.ceb.2009.03.003>

- Stephens, D.J. 2003. De novo formation, fusion and fission of mammalian COPII-coated endoplasmic reticulum exit sites. *EMBO Rep.* 4:210–217. <https://doi.org/10.1038/sj.embor.embor736>
- Szul, T., and E. Sztul. 2011. COPII and COPI traffic at the ER-Golgi interface. *Physiology (Bethesda)*. 26:348–364.
- Tagaya, M., K. Arasaki, H. Inoue, and H. Kimura. 2014. Moonlighting functions of the NRZ (mammalian Dsl1) complex. *Front. Cell Dev. Biol.* 2:25. <https://doi.org/10.3389/fcell.2014.00025>
- Tie, H.C., A. Ludwig, S. Sandin, and L. Lu. 2018. The spatial separation of processing and transport functions to the interior and periphery of the Golgi stack. *eLife*. 7:e41301. <https://doi.org/10.7554/eLife.41301>
- Tripathi, A., Y. Ren, P.D. Jeffrey, and F.M. Hughson. 2009. Structural characterization of Tip20p and Dsl1p, subunits of the Dsl1p vesicle tethering complex. *Nat. Struct. Mol. Biol.* 16:114–123. <https://doi.org/10.1038/nsmb.1548>
- Uemura, T., et al. 2009. p31 deficiency influences endoplasmic reticulum tubular morphology and cell survival. *Mol Cell Biol.* 29:1869–1881. <https://doi.org/10.1128/MCB.01089-08>
- Watson, P., A.K. Townley, P. Koka, K.J. Palmer, and D.J. Stephens. 2006. Sec16 defines endoplasmic reticulum exit sites and is required for secretory cargo export in mammalian cells. *Traffic*. 7:1678–1687. <https://doi.org/10.1111/j.1600-0854.2006.00493.x>

Supplemental material

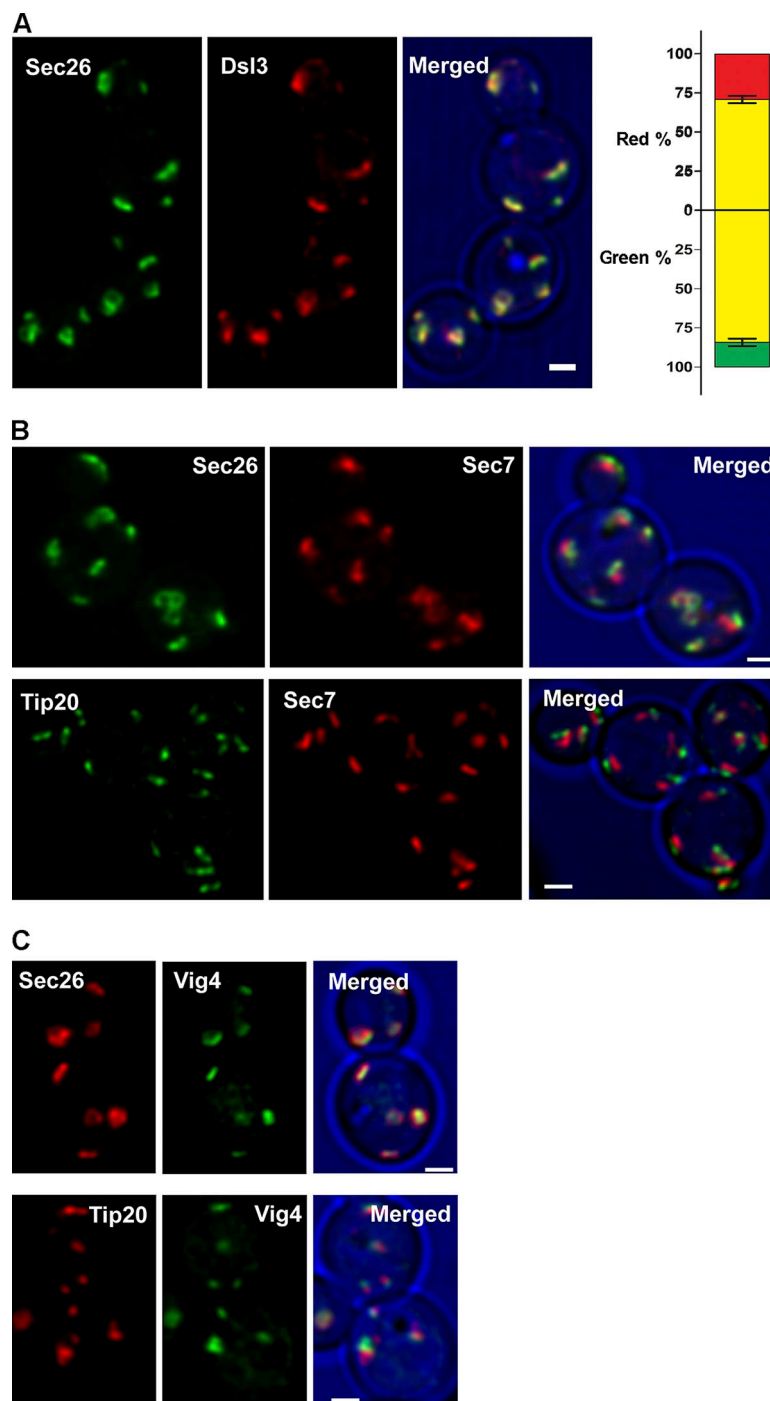


Figure S1. **Localization of Dsl1 complex subunits relative to COPI and Golgi markers. (A)** Colocalization of the COPI marker Sec26 with the Dsl1 complex subunit Dsl3. A strain expressed Sec26-GFP together with Dsl3-mCherry. The overlap between Sec26-GFP and Dsl3-mCherry was quantified as in Fig. 1 C. Scale bar, 1 μ m. **(B)** Localization of the COPI marker Sec26 and the ERAS marker Tip20 relative to the late Golgi marker Sec7. Strains expressed either Sec26-GFP or Tip20-GFP together with Sec7-DsRed. Scale bar, 1 μ m. **(C)** Localization of the COPI marker Sec26 and the ERAS marker Tip20 relative to the early Golgi marker Vig4. Strains expressed either Sec26-mCherry or Tip20-mCherry together with GFP-Vig4. Scale bar, 1 μ m.

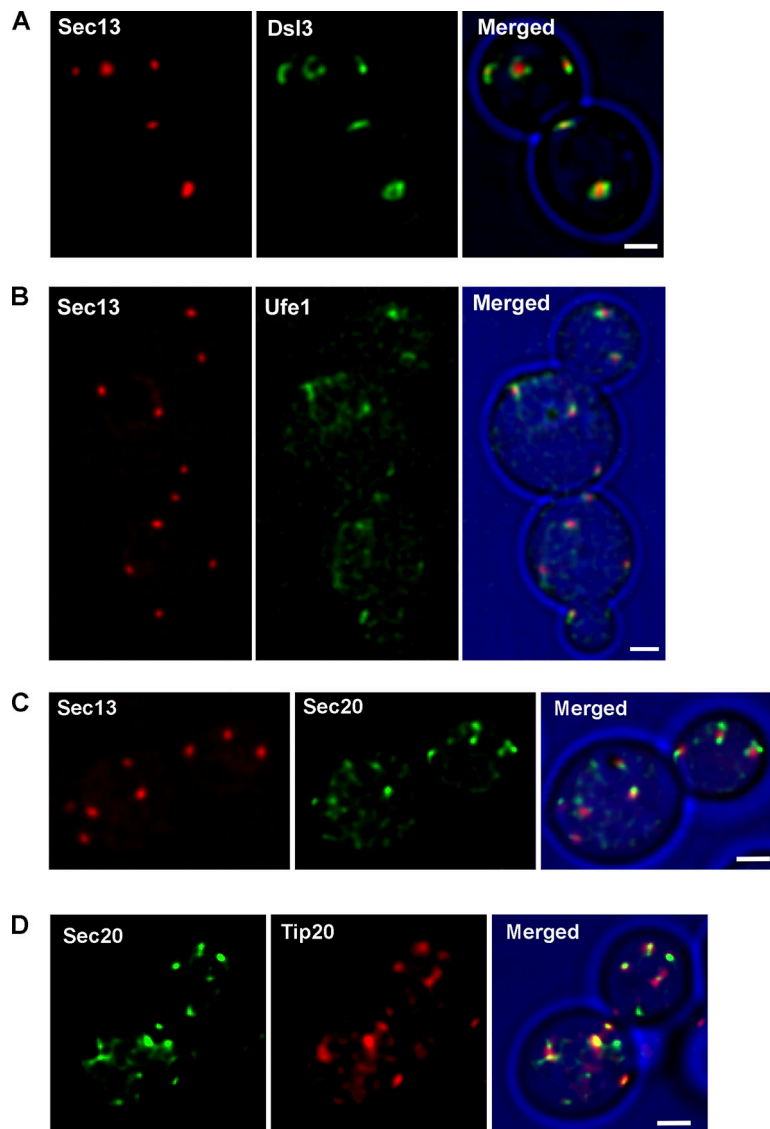


Figure S2. **Visualization of Dsl1 complex subunits and ER-localized SNARES.** **(A)** Localization of the Dsl1 complex subunit Dsl3 relative to the ERES marker Sec13. The strain expressed Sec13-DsRed together with Dsl3-GFP. Scale bar, 1 μ m. **(B)** Localization of the ER-localized SNARE Ufe1 relative to the ERES marker Sec13. The strain expressed Sec13-DsRed together with GFP-Ufe1. Scale bar, 1 μ m. **(C)** Localization of the ER-localized SNARE Sec20 relative to the ERES marker Sec13. The strain expressed Sec13-DsRed together with GFP-Sec20. Scale bar, 1 μ m. **(D)** Relative localizations of the ER-localized SNAREs Sec20 and Tip20. The strain expressed GFP-Sec20 together with Tip20-mCherry. Scale bar, 1 μ m.

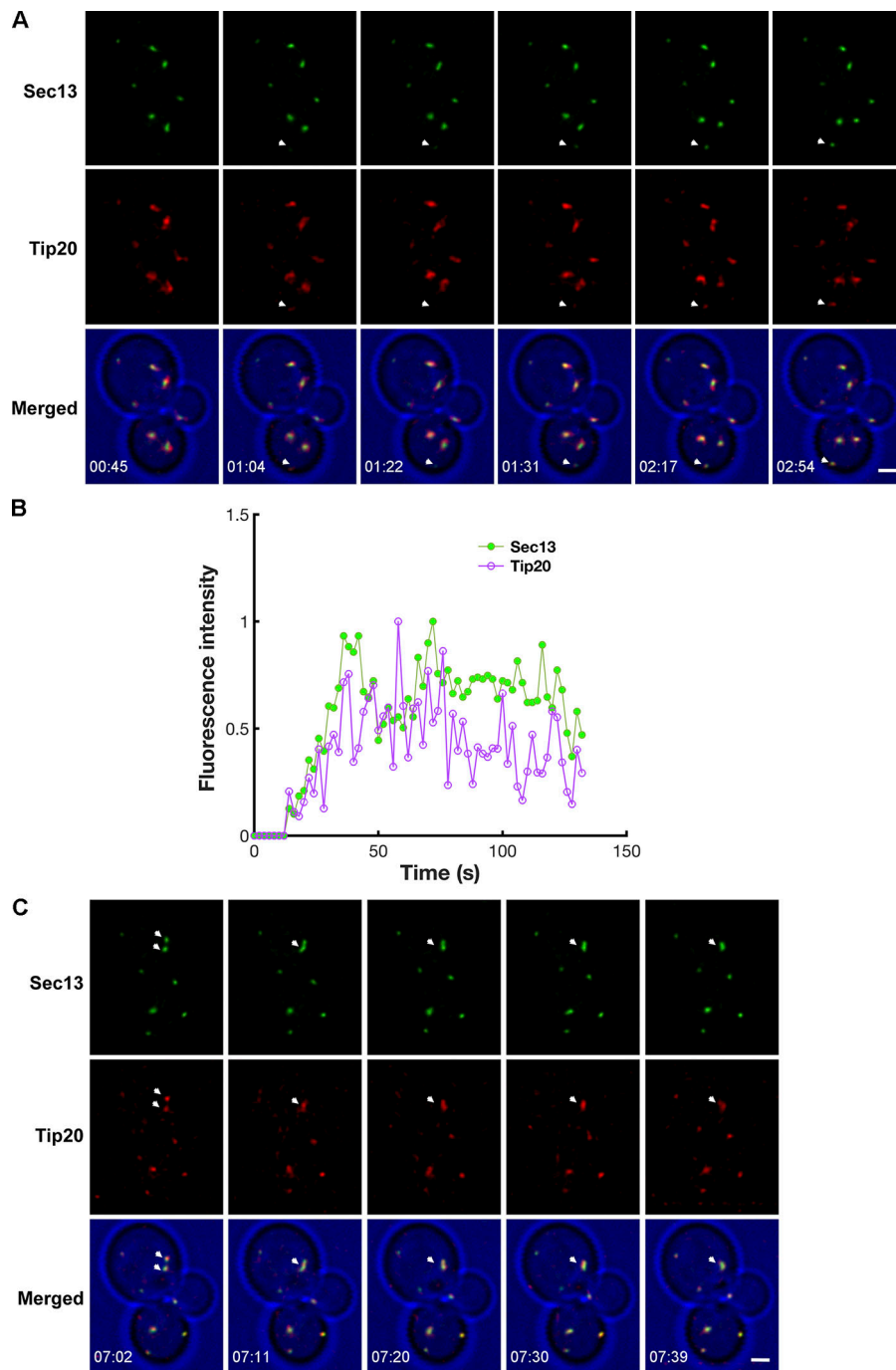


Figure S3. **Coupled dynamics of ERES and ERAS with swapped fluorescent protein tags.** (A) Parallel de novo formation of ERES structures marked with Sec13 and of ERAS structures marked with Tip20. The strain expressed Sec13-GFP together with Tip20-mCherry, using the same marker proteins as in Fig. 3 but swapped fluorescent protein tags. As marked by the arrows, the coupled formation of a new ERES and the associated ERAS were tracked by 4D confocal microscopy. Shown are frames from Video 3. Scale bar, 1 μm . (B) Quantification of the fluorescence signals from the newly formed structures marked by the arrows in A. Each plot was normalized by setting the highest value to 1. (C) Parallel fusion of ERES structures marked with Sec13 and of ERAS structures marked with Tip20. The procedure was as in A, except that the arrows mark two ERES-ERAS pairs that fused to form a single ERES-ERAS pair. Shown are frames from Video 3. Scale bar, 1 μm .

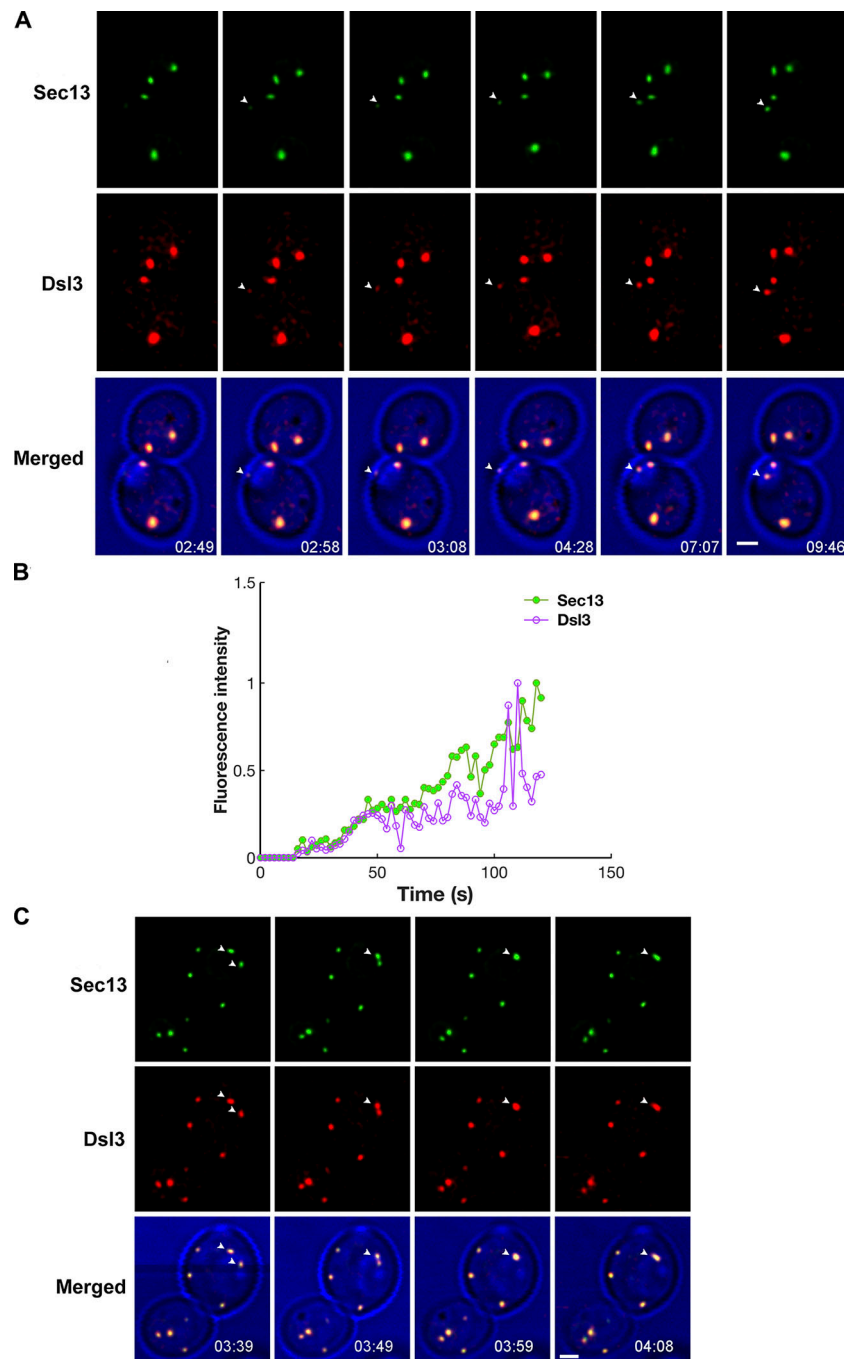


Figure S4. **Coupled formation of ERES and ERAS tracked using Dsl3.** (A) The procedure was as in Fig. S3 A, except that the ERAS marker was Dsl3-mCherry. Shown are frames from Video 4. Scale bar, 1 μm . (B) Quantification of the fluorescence signals from the newly formed structures marked by the arrows in A. Each plot was normalized by setting the highest value to 1. (C) Parallel fusion of ERES structures marked with Sec13 and of ERAS structures marked with Dsl3. The procedure was as in Fig. S3 C, except that the ERAS marker was Dsl3-mCherry. Shown are frames from Video 5. Scale bar, 1 μm .

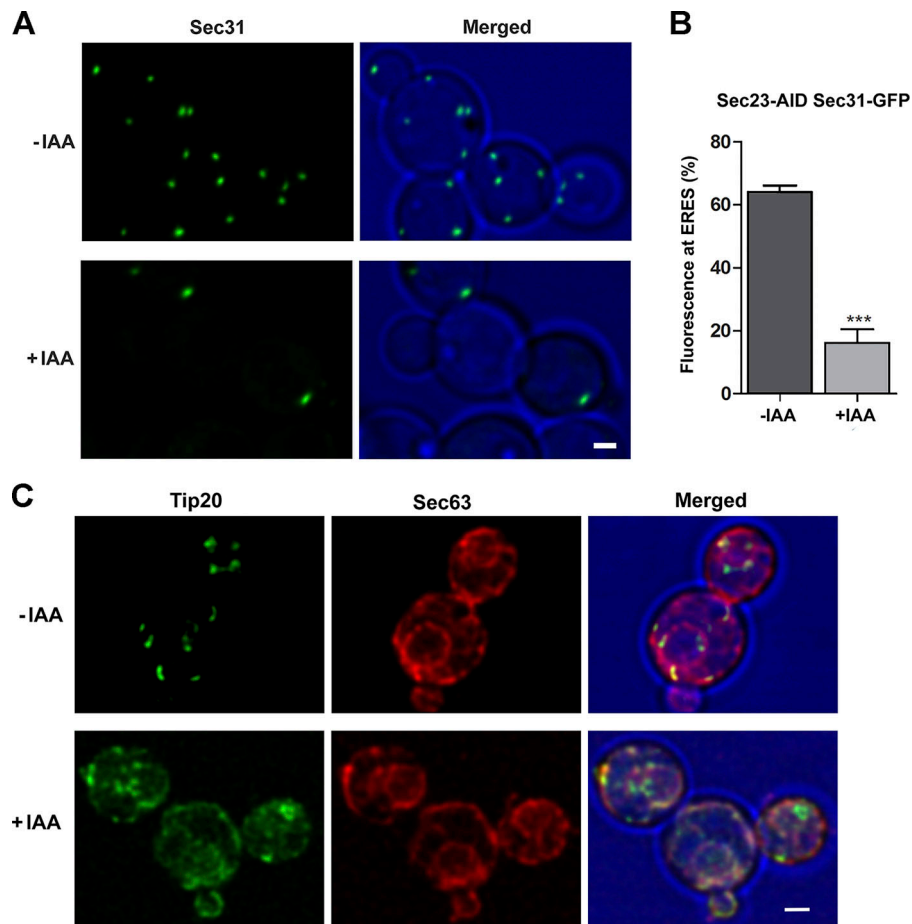


Figure S5. **Effect on ERES and ERAS of inactivating Sec23.** **(A)** Distribution of the ERES marker Sec31 before and after auxin-induced degradation of the COPII inner layer subunit Sec23. A strain expressed Sec31-GFP together with OstTIR1 and Sec23-AID. Images were captured before and after treatment with IAA for 30 min. Scale bar, 1 μ m. **(B)** Quantification of the data from A. The percentage of the total GFP signal that was present at punctate ERES was measured for \sim 30 individual cells in each sample. Bars indicate SEM. Asterisks indicate that the punctate fluorescence in the treated sample was significantly lower at $P < 0.0001$. **(C)** Distribution of the ERAS marker Tip20 relative to the general ER marker Sec63 before and after auxin-induced degradation of the COPII inner layer subunit Sec23. A strain expressed Tip20-GFP together with Sec63-mCherry as well as OstTIR1 and Sec23-AID. Images were captured before and after treatment with IAA for 30 min. Scale bar, 1 μ m.

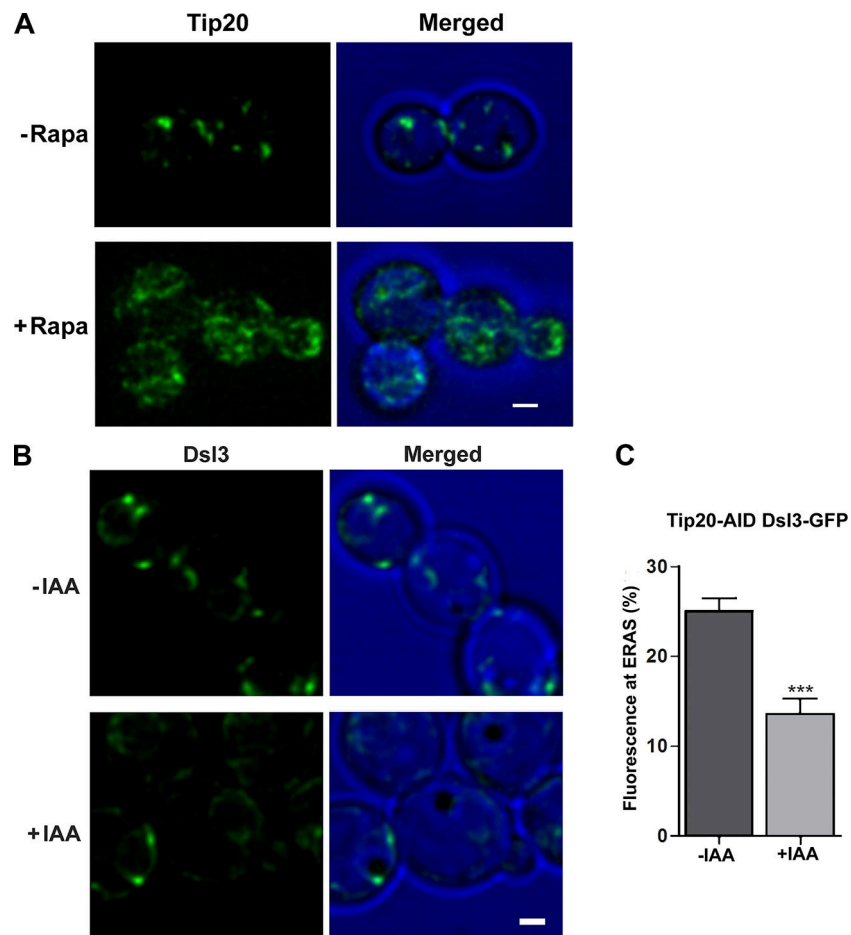


Figure S6. **Control experiments to verify inactivation of the ERAS component Tip20.** **(A)** Redistribution of FRB-tagged Tip20 by the anchor-away procedure. A strain expressed Tip20-GFP-FRB together with the Rpl17-FKBPx4 ribosomal anchor. Images were captured before and after treatment with rapamycin (Rapa) for 10 min. Scale bar, 1 μ m. **(B)** Distribution of the Dsl1 complex subunit Dsl3 before and after auxin-induced degradation of Tip20. A strain expressed Dsl3-GFP together with OsTIR1 and Tip20-AID. Images were captured before and after treatment with IAA for 30 min. Scale bar, 1 μ m. **(C)** Quantification of the data from B. The percentage of the total GFP signal that was present at punctate ERAS was measured for 30 individual cells in each sample. Bars indicate SEM. Asterisks indicate statistical significance at ***, $P < 0.0001$.

Video 1. **De novo formation of ERES and ERAS.** *P. pastoris* cells expressing Tip20-GFP (ERAS) and Sec13-DsRed (ERES) were imaged by 4D confocal microscopy. The fluorescence data for each time point were projected and merged with a transmitted light image of the cells. Time is indicated in minute:second format, and the frame rate is 5 frames per second. Frames from this video are shown in Fig. 3 A.

Video 2. **Fusion of ERES and ERAS.** *P. pastoris* cells expressing Tip20-GFP (ERAS) and Sec13-DsRed (ERES) were imaged by 4D confocal microscopy. The fluorescence data for each time point were projected and merged with a transmitted light image of the cells. Time is indicated in minute:second format, and the frame rate is 5 frames per second. Frames from this video are shown in Fig. 3 C.

Video 3. **De novo formation and fusion of ERES and ERAS with swapped fluorescence protein tags.** The procedure was as in Video 1 and Video 2, except that the *P. pastoris* cells expressed Tip20-mCherry (ERAS) and Sec13-GFP (ERES). Frames from this video are shown in Fig. S3, A and C, and the frame rate is 5 frames per second.

Video 4. **De novo formation of ERES and ERAS visualized with alternative markers.** The procedure was as in Video 1, except that the *P. pastoris* cells expressed Sec13-GFP (ERES) and Dsl3-mCherry (ERAS). Frames from this video are shown in Fig. S4 A, and the frame rate is 5 frames per second.

Video 5. **Fusion of ERES and ERAS visualized with alternative markers.** The procedure was as in [Video 2](#), except that the *P. pastoris* cells expressed Sec13-GFP (ERES) and Dsl3-mCherry (ERAS). Frames from this video are shown in [Fig. S4 C](#), and the frame rate is 5 frames per second.

Provided online are two tables. Table S1 lists plasmid constructs. Table S2 lists *P. pastoris* strains.